Computer Methods in Applied Mechanics and Engineering 419 (2024) 116667

Contents lists available at ScienceDirect

Comput. Methods Appl. Mech. Engrg.

journal homepage: www.elsevier.com/locate/cma

A unified analytical expression of the tangent stiffness matrix of holonomic constraints

Chao Peng, Alessandro Tasora, Dario Fusai, Dario Mangoni *

University of Parma, Department of Industrial Engineering, Parco Area delle Scienze 181/A, Parma, 43121, PR, Italy

GRAPHICAL ABSTRACT

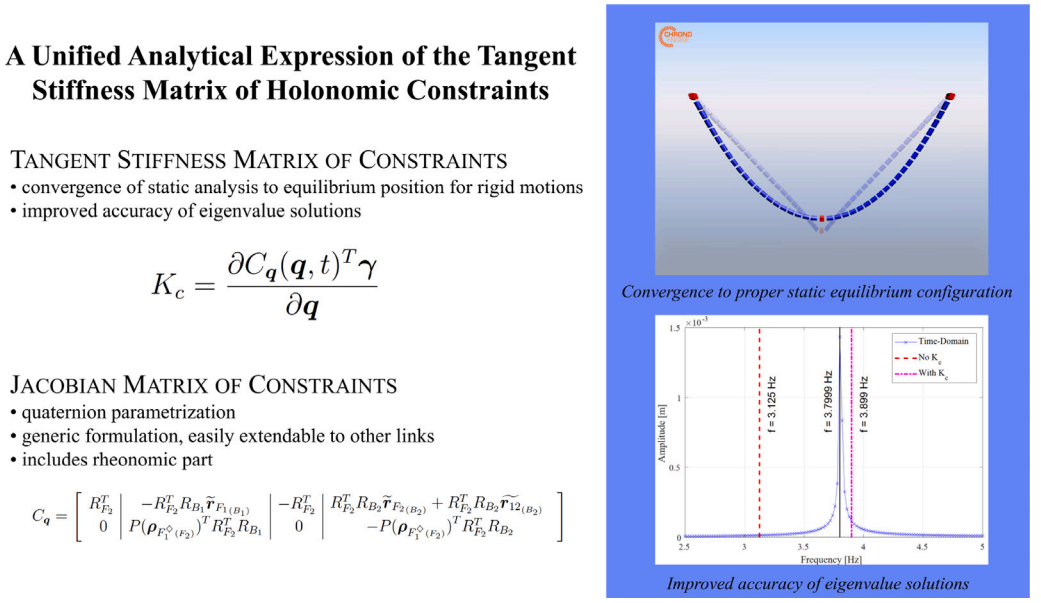

ARTICLE INFO

Keywords:
Tangent stiffness matrix of constraints
Holonomic constraint
Linearization
Eigenvalue analysis

ABSTRACT

While an accurate computation of the tangent stiffness matrix of multibody systems is usually of critical importance in various numerical analyses, one contribution often neglected in dynamics is represented by the *tangent stiffness matrix of constraints*. This term, resulting from the change of joints reactions with respect to the coordinates of the connected bodies, is indeed easily discarded for the sake of performance due to its slight effect on dynamic simulation results. On

* Corresponding author.
E-mail addresses: chao.peng@unipr.it (C. Peng), alessandro.tasora@unipr.it (A. Tasora), dario.fusai@unipr.it (D. Fusai), dario.mangoni@unipr.it (D. Mangoni).
URL: https://digitaldynamicslab.unipr.it/ (A. Tasora).

https://doi.org/10.1016/j.cma.2023.116667
Received 31 July 2023; Received in revised form 31 October 2023; Accepted 23 November 2023
Available online 25 November 2023

the contrary, it plays a critical role when static or eigenvalue analyses are required, especially for those cases featuring free motions. While the topic of holonomic constraint equations and their respective Jacobian matrix is not new in literature, this article aims to provide a general and unified formulation based on quaternion parametrization together with a consistent analytical expression of the tangent stiffness matrix derived through linearization. The article includes also the rheonomic contribution to holonomic constraints. The formulations presented in this work are built on a mixed-basis formulation, in use in many engineering applications, and allow to easily derive specialized versions (e.g. revolute, cylindrical, prismatic joints, etc.) from the same equation set. Examples demonstrate the doubly-positive effect of this additional stiffness term: first, static analyses are able to converge to the actual equilibrium position and second, the eigenvalues analyses proved to be more consistent. For this latter set of tests the non-linear dynamic results, observed in the frequency domain, are compared against those coming from eigenvalue analysis, in order to prove the augmented accuracy of the results.

1. Introduction

The tangent stiffness matrix plays a key role in the formulation and solution of any multibody system since it contains various fundamental terms coming from the linearization of the inertial, external and internal forces with respect to the generalized coordinates. However, each term might have a varying influence depending on the type of the analysis conducted and of the system under examination. In most multi-flexible-body systems, for example, the structural stiffness matrix K_f together with the inertial stiffness matrix K_i usually are the main driving terms, thus often justifying the omission of other negligible contributions, like the constraint stiffness matrix K_c, coming from the linearization of the reaction forces of the joints [1]. This latter matrix, on the contrary, becomes very relevant in case of extremely-soft flexible bodies or especially in rigid-body systems: in fact, differently from the stiffness property provided by the material of the joints [2], this matrix does not come from the deformation of bodies, but from the change in direction of the reaction forces and torques in the joints.

A typical example consists in a pendulum hinged to a fixed point and subject to gravity: if the tangent stiffness matrix of constraints is not considered, the system stiffness matrix is zero. It follows that, in the Newton–Raphson iteration required by the non-linear static analysis, the method does not know the potential correct direction to search for the equilibrium state, thus leading to divergence. Moreover, the eigenvalues would be zero-valued because of the zero stiffness matrix: this is incorrect since it is well known that the pendulum has an oscillatory motion at the equilibrium state.

On the contrary, it is true that the very same model can be easily simulated in dynamic mode without the stiffness matrix of constraints: this is because dynamic simulations can still converge to proper solutions even with just an approximation of the stiffness matrix [3]. However, even in this scenario where iterative schemes still observe progressive refinements, the presence of the stiffness matrix of constraints could increase stability, convergence and in some cases also the performance of numerical methods: in computer graphics applications, for example in movies and game industries where performance has a higher priority over accuracy, its introduction can effectively improve the stability of the dynamic solution [4] especially for systems involving inextensible objects and articulated chains. There, the symmetric form $\left(K_c + K_c{}^T\right)/2$ is employed to preserve the matrix symmetry in the implicit integrator resulting in a speed boost in the solution of linear equations. Inspired by the discovery of Tournier [4], Andrews [5] developed a diagonal approximation of the tangent stiffness matrix of constraints to alleviate the energy dissipation in the simulation, and derived the closed-form expressions for a library of joints commonly used in articulated rigid body simulations, however no unified expression is offered.

Macklin [6] further built the diagonal approximation of K_c through successive finite differences using the last two Newton iterations and clamped the shift to guarantee the matrix positive definiteness.

While many research works [1,7,8] in the field of linearization of the equations of motion of constrained multibody systems have pointed out the existence of the tangent stiffness matrix of constraints, no explicit expressions have been clearly reported.

Bauchau [9] introduced the tangent stiffness matrix (called *equivalent stiffness matrix* in his book), but based on Euler and not quaternion parametrization. Also the contribution of Géradin and Cardona [10] refers to tangent stiffness matrices of constraints, but it misses to provide a detailed expansion of this term. Minaker [11] derived the analytical expressions of the tangent stiffness matrix for the revolute joint, the point-on-plane contact and the rolling disk contact, and revealed the significant influence of the tangent stiffness matrices of constraint on the eigenvalues of the A-arm suspension system, which demonstrated its importance in the vehicle dynamics analysis. In the end, the author stated that there might exist a generic expression for the tangent stiffness matrix of constraints because of the similarities between the forms of the stiffness matrix for the studied constraints. Minaker [12] calculated the tangent stiffness matrix of a constant velocity joint and verified it through comparison between different modelling approaches.

To the best of the authors' knowledge a general, analytical and explicit expression of the tangent stiffness matrix of holonomic constraints, including the rheonomic part, is still missing in the literature.

In this work, the constraint equation $\boldsymbol{C}(\boldsymbol{q}, t) = \boldsymbol{0}$ of holonomic constraints is proposed and later used to compute the Jacobian matrix C_q. A consistent and unified analytical formulation of the tangent stiffness matrix of holonomic constraints is then obtained. In Section 2 the dynamic equation of motion is introduced together with the constraints equations. Scleronomic (Section 2.1) and rheonomic formulations (Section 2.2) for the Jacobian matrices are offered, followed by the computation of the tangent stiffness matrix of constraints for both joint types in Section 3. Three examples are then introduced in Section 4 to demonstrate its application in the static and eigenvalue analysis of the multibody systems with rigid motions. Relevant properties and notations can be found in appendices (Appendices A–C).

2. Jacobian matrix of constraints

For simple mechanical systems, one may write the *Ordinary Differential Equation* (ODE) of motion by carefully choosing the independent coordinates. When the system includes more bodies and connection joints, it becomes difficult to determine the independent coordinates, often not even unique [13].

To overcome this issue, the index-3 Lagrange multiplier method has been developed and widely used in the field of multibody dynamics. The fundamental idea is to set up the ODE of all rigid bodies and flexible elements with the assumption that they are completely separated. The ODE of every single object is set up by using the *Newton-Euler* formulation because of the advantage of easier mathematical derivation and higher computational efficiency. To this redundant set of coordinates, constraints are added, thus leading to Differential-Algebraic Equations system (DAE). In our formulation, we assume that the translational coordinates are described in the *absolute* frame while the rotational coordinates are expressed in the *local* frame of the object; we call it a *mixed-basis* formalism. This choice, though arbitrary, is motivated by the simpler form that rotational equations assume [14].

The constraint conditions

$$\boldsymbol{C}(\boldsymbol{q}, \dot{\boldsymbol{q}}, t) = \boldsymbol{0} \tag{1}$$

consist in a vector of n_c scalar equations of generalized coordinates (positions, rotations) $\boldsymbol{q}$, of velocities $\dot{\boldsymbol{q}}$, of time t.

In case of *holonomic* constraints (i.e. not depending on velocities $\dot{\boldsymbol{q}}$), that is the most common practical situation, the conditions are simplified to:

$$\boldsymbol{C}(\boldsymbol{q}, t) = \boldsymbol{0} \tag{2}$$

The vector constraint equation is linearized as:

$$\delta\boldsymbol{C}(\boldsymbol{q}, t) = C_q \delta\boldsymbol{q} + \boldsymbol{C}_t \delta t \tag{3}$$

by introducing the following symbols:

$$C_q := \frac{\partial \boldsymbol{C}}{\partial \boldsymbol{q}} \quad \in \mathbb{R}^{n_c \times n_q} \tag{4}$$

$$\boldsymbol{C}_t := \frac{\partial \boldsymbol{C}}{\partial t} \quad \in \mathbb{R}^{n_c} \tag{5}$$

where C_q is the so-called *Jacobian matrix of constraints*.

The reaction forces and torques in the joints are added to the Newton-Euler equations to formulate the complete equations of motion, which are expressed as the following index-3 *Differential Algebraic Equation* (DAE),

$$\begin{cases} M(\boldsymbol{q})\ddot{\boldsymbol{q}} + C_q(\boldsymbol{q}, t)^T \boldsymbol{\gamma} = \boldsymbol{f}(\boldsymbol{q}, \dot{\boldsymbol{q}}, t) - \boldsymbol{f}_g(\boldsymbol{q}, \dot{\boldsymbol{q}}) & \text{(a)} \\ \boldsymbol{C}(\boldsymbol{q}, t) = \boldsymbol{0} & \text{(b)} \end{cases} \tag{6}$$

where $\boldsymbol{f}$ is the vector of external and internal forces, $\boldsymbol{f}_g$ represents the gyroscopic and centrifugal components of the inertial forces, where the full inertial forces are $\boldsymbol{f}_i = M\ddot{\boldsymbol{q}} + \boldsymbol{f}_g$ and $\boldsymbol{\gamma}$ are the Lagrange multipliers.

Linearizing the DAE about the equilibrium point one obtains [1]

$$\begin{cases} M(\boldsymbol{q})\delta\ddot{\boldsymbol{q}} + D(\boldsymbol{q}, \dot{\boldsymbol{q}}, t)\delta\dot{\boldsymbol{q}} + K(\boldsymbol{q}, \dot{\boldsymbol{q}}, \ddot{\boldsymbol{q}}, \boldsymbol{\gamma}, t)\delta\boldsymbol{q} + C_q(\boldsymbol{q}, t)^T \delta\boldsymbol{\gamma} = \boldsymbol{0} & \text{(a)} \\ C_q(\boldsymbol{q}, t)\delta\boldsymbol{q} = \boldsymbol{0} & \text{(b)} \end{cases} \tag{7}$$

where the *damping matrix of the system* is

$$D(\boldsymbol{q}, \dot{\boldsymbol{q}}, t) = -\frac{\partial \boldsymbol{f}(\boldsymbol{q}, \dot{\boldsymbol{q}}, t)}{\partial \dot{\boldsymbol{q}}} + \frac{\partial \boldsymbol{f}_g(\boldsymbol{q}, \dot{\boldsymbol{q}})}{\partial \dot{\boldsymbol{q}}} \tag{8}$$

and the tangent stiffness matrix of the system $K(\boldsymbol{q}, \dot{\boldsymbol{q}}, \ddot{\boldsymbol{q}}, \boldsymbol{\gamma}, t)$ can be expanded as

$$K(\boldsymbol{q}, \dot{\boldsymbol{q}}, \ddot{\boldsymbol{q}}, \boldsymbol{\gamma}, t) = \frac{\partial (M(\boldsymbol{q})\ddot{\boldsymbol{q}} + \boldsymbol{f}_g)}{\partial \boldsymbol{q}} + \frac{\partial C_q(\boldsymbol{q}, t)^T}{\partial \boldsymbol{q}}\boldsymbol{\gamma} - \frac{\partial \boldsymbol{f}(\boldsymbol{q}, \dot{\boldsymbol{q}}, t)}{\partial \boldsymbol{q}} \tag{9}$$

In particular, the *tangent stiffness matrix of constraints* term consists is:

$$K_c = \frac{\partial C_q(\boldsymbol{q}, t)^T}{\partial \boldsymbol{q}}\boldsymbol{\gamma} \tag{10}$$

It is then clear that, in order to compute this term, the analytical formulation of the Jacobian matrix of constraints is needed. In the following section its expression is offered, for both *scleronomic* and *rheonomic* constraints.

2.1. Scleronomic constraints

Suppose a holonomic-scleronomic constraint (i.e. not depending explicitly on time) is used to connect two rigid bodies whose reference frames are B_1 and B_2 respectively. In this case the constraints equations depend, by definition, only on the system configuration i.e. $C(\boldsymbol{q}) = 0$, thus loosing the dependency over time. Two auxiliary joint frames F_1 and F_2, attached respectively to the two bodies, are introduced (Fig. 1). Throughout the paper body 1 will be considered the *driven* body, while body 2 has to

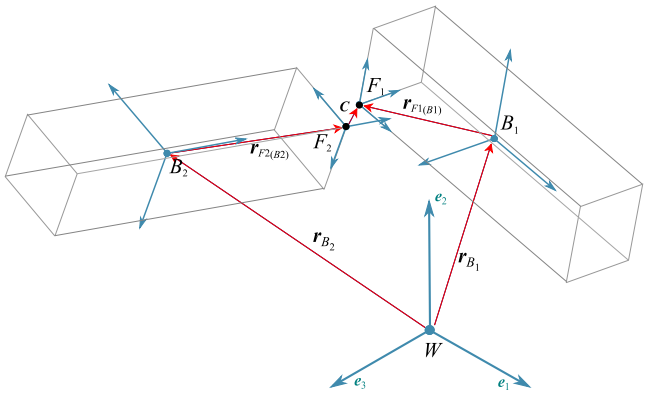

Fig. 1. The main frame F_2 and the driven frame F_1 for a holonomic-scleronomic constraint. In this figure the constraint is not exactly satisfied, hence a small clearance c is shown.

be considered the *main* body since it is the one with respect to which constraint equations are written. The absolute positions and rotations of the two bodies $\boldsymbol{r}_{B_1}$, R_{B_1}, $\boldsymbol{r}_{B_2}$, R_{B_2} are functions of generalized coordinates $\boldsymbol{q}$. The body-relative positions and rotations of the two joint frames F_1, F_2 are constant geometric properties, namely $\boldsymbol{r}_{F_{1(B_1)}}$, $R_{F_{1(B_1)}}$, $\boldsymbol{r}_{F_{2(B_2)}}$, $R_{F_{2(B_2)}}$.

The constraint equations can be expressed in an arbitrary frame. Since in engineering practice the reaction forces and torques are typically described or measured in the local basis of the joint, we choose to use the basis of the main frame F_2 so that the reaction forces and torques are consistent with the intuitive understanding.

2.1.1. Translational scleronomic constraints

In the following, we use the notation $\boldsymbol{r}_{A_{(F)}}$ to indicate the position of a point A with respect to a floating frame F, expressed in the basis of F. When the basis is the absolute reference, we use the letter W, or we omit it. Similarly, with $R_{F_{(G)}}$ we define the rotation matrix $R \in \mathrm{SO3}$ of a frame F with respect to a frame G, that can be omitted when $G \equiv W$.

In order to constrain the relative displacement between the two frames, the positions of the origins of F_1 and F_2 should be made coincident. This can be done by imposing the condition $\boldsymbol{r}_{F_{1(F_2)}} - \boldsymbol{r}_{F_{2(F_2)}} = \boldsymbol{r}_{F_{1(F_2)}} = \boldsymbol{0}$. The constraint equation becomes

$$\boldsymbol{C}(\boldsymbol{q}) = \boldsymbol{r}_{F_{1(F_2)}} = \boldsymbol{0} \tag{11}$$

Using the point transformation $\boldsymbol{r}_{F_{(W)}} = \boldsymbol{r}_{B_{(W)}} + R_B \boldsymbol{r}_{F_{(B)}}$ and omitting the (W) basis subscript for variables in absolute coordinates, we expand the terms and obtain

$$\boldsymbol{C}(\boldsymbol{q}) = R_{F_2}^T \left(\boldsymbol{r}_{B_1} + R_{B_1} \boldsymbol{r}_{F_{1(B_1)}} - \boldsymbol{r}_{B_2} - R_{B_2} \boldsymbol{r}_{F_{2(B_2)}} \right) = \boldsymbol{0} \tag{12}$$

The Jacobian matrix of the constraint $C_{\boldsymbol{q}}$ is a sparse matrix with four row blocks, and it can be computed by showing the dependence of the variation $\delta \boldsymbol{C}(\boldsymbol{q})$ from the four variation blocks $\delta \boldsymbol{r}_{B_1}$, $\boldsymbol{\theta}^{\delta}_{l_{B_1}}$, $\delta \boldsymbol{r}_{B_2}$, $\boldsymbol{\theta}^{\delta}_{l_{B_2}}$ in the vector of generalized variations $\delta \boldsymbol{q}$

$$\begin{aligned}
\delta \boldsymbol{C}(\boldsymbol{q}) =& \delta R_{F_2}^T \left(\boldsymbol{r}_{B_1} + R_{B_1} \boldsymbol{r}_{F_{1(B_1)}} - \boldsymbol{r}_{B_2} - R_{B_2} \boldsymbol{r}_{F_{2(B_2)}} \right) + R_{F_2}^T \delta \left(\boldsymbol{r}_{B_1} + R_{B_1} \boldsymbol{r}_{F_{1(B_1)}} - \boldsymbol{r}_{B_2} - R_{B_2} \boldsymbol{r}_{F_{2(B_2)}} \right) \\
=& \delta \left(R_{F_{2(B_2)}}^T R_{B_2}^T \right) \left(\boldsymbol{r}_{B_1} + R_{B_1} \boldsymbol{r}_{F_{1(B_1)}} - \boldsymbol{r}_{B_2} - R_{B_2} \boldsymbol{r}_{F_{2(B_2)}} \right) + R_{F_2}^T \left(\delta \boldsymbol{r}_{B_1} + \delta (R_{B_1} \boldsymbol{r}_{F_{1(B_1)}}) - \delta \boldsymbol{r}_{B_2} - \delta (R_{B_2} \boldsymbol{r}_{F_{2(B_2)}}) \right) \\
=& R_{F_{2(B_2)}}^T \delta R_{B_2}^T \left(\boldsymbol{r}_{F_1.F_2} \right) + R_{F_2}^T \left(\delta \boldsymbol{r}_{B_1} + \delta R_{B_1} \boldsymbol{r}_{F_{1(B_1)}} - \delta \boldsymbol{r}_{B_2} - \delta R_{B_2} \boldsymbol{r}_{F_2(B_2)} \right) \\
=& R_{F_{2(B_2)}}^T \widetilde{\theta}^{\delta T}_{l_{B_2}} R_{B_2}^T \boldsymbol{r}_{F_1.F_2} + R_{F_2}^T \left(\delta \boldsymbol{r}_{B_1} + R_{B_1} \widetilde{\theta}^{\delta}_{l_{B_1}} \boldsymbol{r}_{F_{1(B_1)}} - \delta \boldsymbol{r}_{B_2} - R_{B_2} \widetilde{\theta}^{\delta}_{l_{B_2}} \boldsymbol{r}_{F_{2(B_2)}} \right) \\
=& R_{F_{2(B_2)}}^T \widetilde{r12}_{(B_2)} \boldsymbol{\theta}^{\delta}_{l_{B_2}} + R_{F_2}^T \left(\delta \boldsymbol{r}_{B_1} - R_{B_1} \widetilde{\boldsymbol{r}}_{F_{1(B_1)}} \boldsymbol{\theta}^{\delta}_{l_{B_1}} - \delta \boldsymbol{r}_{B_2} + R_{B_2} \widetilde{\boldsymbol{r}}_{F_{2(B_2)}} \boldsymbol{\theta}^{\delta}_{l_{B_2}} \right) \\
=& R_{F_2}^T R_{B_2} \widetilde{r12}_{(B_2)} \boldsymbol{\theta}^{\delta}_{l_{B_2}} + R_{F_2}^T \left(\delta \boldsymbol{r}_{B_1} - R_{B_1} \widetilde{\boldsymbol{r}}_{F_{1(B_1)}} \boldsymbol{\theta}^{\delta}_{l_{B_1}} - \delta \boldsymbol{r}_{B_2} + R_{B_2} \widetilde{\boldsymbol{r}}_{F_{2(B_2)}} \boldsymbol{\theta}^{\delta}_{l_{B_2}} \right)
\end{aligned} \tag{13}$$

where $\widetilde{\boldsymbol{a}}$ denotes the 3×3 skew-symmetric matrix associated with the vector $\boldsymbol{a}$. We also considered the properties $\delta R = R \widetilde{\theta}^{\delta}_{l}$ and $\widetilde{\boldsymbol{a}}^T = -\widetilde{\boldsymbol{a}}$, $\widetilde{\boldsymbol{a}}\boldsymbol{b} = -\widetilde{\boldsymbol{b}}\boldsymbol{a}$, $\forall \boldsymbol{a}, \boldsymbol{b} \in \mathbb{R}^3$. Moreover, for the sake of notation compactness, we grouped the vector from F_1 to F_2 expressed in the B_2 frame into:

$$\boldsymbol{r}_{12_{(B_2)}} = R_{B_2}^T \boldsymbol{r}_{F_1.F_2} = R_{B_2}^T \left(\boldsymbol{r}_{B_1} + R_{B_1} \boldsymbol{r}_{F_{1(B_1)}} - \boldsymbol{r}_{B_2} - R_{B_2} \boldsymbol{r}_{F_{2(B_2)}} \right) \tag{14}$$

Finally, recalling Eq. (3), one can group the terms and write the four blocks in the sparse Jacobian matrix $C_{\boldsymbol{q}}$ for the translational constraint as

$$C_{\boldsymbol{q}}(\boldsymbol{q}) = \left[\begin{array}{c|c|c|c} R_{F_2}^T & -R_{F_2}^T R_{B_1} \widetilde{\boldsymbol{r}}_{F_{1(B_1)}} & -R_{F_2}^T & R_{F_2}^T R_{B_2} \widetilde{\boldsymbol{r}}_{F_{2(B_2)}} + R_{F_2}^T R_{B_2} \widetilde{r12}_{(B_2)} \end{array} \right] \tag{15}$$

2.1.2. Rotational scleronomic constraints

We choose to parametrize the finite rotation using quaternions because it does not exhibit singularities. The constraints on the rotational DOFs are expressed based on the quaternion algebra. In Appendix B a list of useful properties are offered.

The four components of a unit quaternion $\boldsymbol{\rho}$ can be interpreted as the elements of *Euler parameters* $\boldsymbol{e} = \left[e_0, e_1, e_2, e_3\right]^T$ [9]

$$\begin{aligned} e_0 &= \cos(\theta/2) & e_1 &= n_x \sin(\theta/2) \\ e_2 &= n_y \sin(\theta/2) & e_3 &= n_z \sin(\theta/2) \end{aligned} \tag{16}$$

which describe a finite rotation about the spinning axis $\boldsymbol{n} = \left[n_x, n_y, n_z\right]^T$ by the angle θ. Thus the imaginary part of a unit quaternion $\boldsymbol{\rho}$ maps the three rotational DOFs. This turns out to be useful also to retrieve relative angles of constrained frames: considering for example a revolute joint along x axis, the relative rotation can be expressed as one of the following:

$$\theta = 2 \arccos\left(e_0\right) \tag{17a}$$

$$\theta = 2 \arctan2\left(\frac{e_1}{n_x}, e_0\right) \tag{17b}$$

Remembering the implicit constraint of the unit quaternion: $\|\boldsymbol{\rho}\| = \sqrt{\rho_0^2 + \rho_1^2 + \rho_2^2 + \rho_3^2} = 1$, only its imaginary part $\boldsymbol{\rho}$ is required to formulate the constraint equation $\boldsymbol{C}(\boldsymbol{q})$ for the three rotational DOFs. It has to be noted that the unit norm of the quaternion, while it could be explicitly enforced by a constraint, is usually guaranteed by the integration scheme, that should appropriately update the quaternion through an exponential update [14] such as:

$$\boldsymbol{\rho}^{(t+\Delta t)} = \boldsymbol{\rho}^{(t)} \left[\cos\left(\frac{1}{2}\|\boldsymbol{\omega}_l\|\Delta t\right), \ \frac{\boldsymbol{\omega}_l}{\|\boldsymbol{\omega}_l\|} \sin\left(\frac{1}{2}\boldsymbol{\omega}_l \Delta t\right)\right]$$

To constrain the relative rotation between two frames F_1 and F_2, the constraint equation is given as:

$$\boldsymbol{C}(\boldsymbol{q}) = \mathrm{Im}\left(\boldsymbol{\rho}_{F_{1\,(F_2)}}\right) = \boldsymbol{0}_{3\times 1} \tag{18}$$

where $\mathrm{Im}\,(\cdot)$ is the operator to extract the imaginary vectorial part of a quaternion.

Instead of using all the four components of $\boldsymbol{\rho}_{F_{1\,(F_2)}}$ to define the rotational constraint equation, which complicates the mathematical formulation of the Jacobian matrix [15], it is indeed sufficient to constrain only its imaginary part.

Remembering the formula (C.2) (see Appendix C for specific notation and definitions) the variation of the constraint equation (18) is differentiated as:

$$\delta\boldsymbol{C}(\boldsymbol{q}) = \mathrm{Im}\left(\delta\boldsymbol{\rho}_{F_{1\,(F_2)}}\right) = P(\boldsymbol{\rho}_{F_{1\,(F_2)}})\boldsymbol{\theta}^{\delta}_{l_{F_1}(F_2)} \tag{19}$$

The relative virtual rotation vector $\boldsymbol{\theta}^{\delta}_{l_{F_1}(F_2)}$ of the frame F_1 with respect to the frame F_2 can be calculated through deriving the variation of the corresponding rotation tensor $\delta R_{F_{1\,(F_2)}}$.

The relative rotation tensor can be expanded as $R_{F_{1\,(F_2)}} = R^T_{F_{2\,(B_2)}} R^T_{B_2} R_{B_1} R_{F_{1\,(B_1)}}$. Its variation is calculated as:

$$\delta R_{F_{1\,(F_2)}} = R^T_{F_{2\,(B_2)}} \left(-\widetilde{\boldsymbol{\theta}^{\delta}_{l\,B_2}} R^T_{B_2} R_{B_1} + R^T_{B_2} R_{B_1} \widetilde{\boldsymbol{\theta}^{\delta}_{l\,B_1}}\right) R_{F_{1\,(B_1)}} \tag{20}$$

Substituting (20) into $\widetilde{\boldsymbol{\theta}^{\delta}_{l\,F_1\,(F_2)}} = R^T_{F_{1\,(F_2)}} \delta R_{F_{1\,(F_2)}}$, after some calculations and extracting the spinning vectors of the skew-symmetric matrices, one obtains:

$$\boldsymbol{\theta}^{\delta}_{l_{F_1}(F_2)} = R^T_{F_1} \left(R_{B_1} \boldsymbol{\theta}^{\delta}_{l_{B_1}} - R_{B_2} \boldsymbol{\theta}^{\delta}_{l_{B_2}}\right) \tag{21}$$

Substituting (21) into (19), the variation of the constraint equation of rotational DOFs is obtained as:

$$\delta\boldsymbol{C}(\boldsymbol{q}) = P(\boldsymbol{\rho}_{F_{1\,(F_2)}}) R^T_{F_1} \left(R_{B_1} \boldsymbol{\theta}^{\delta}_{l_{B_1}} - R_{B_2} \boldsymbol{\theta}^{\delta}_{l_{B_2}}\right) \tag{22}$$

Remembering (C.4), we can restate the previous relation with respect to the main frame F_2 as:

$$\delta\boldsymbol{C}(\boldsymbol{q}) = P(\boldsymbol{\rho}_{F_{1\,(F_2)}})^T R^T_{F_2} \left(R_{B_1} \boldsymbol{\theta}^{\delta}_{l_{B_1}} - R_{B_2} \boldsymbol{\theta}^{\delta}_{l_{B_2}}\right) \tag{23}$$

Eventually, the Jacobian matrix $C_{\boldsymbol{q}}$ for the rotational DOFs becomes:

$$C_{\boldsymbol{q}}(\boldsymbol{q}) = \left[\begin{array}{c|c|c|c} 0 & P(\boldsymbol{\rho}_{F_{1\,(F_2)}})^T R^T_{F_2} R_{B_1} & 0 & -P(\boldsymbol{\rho}_{F_{1\,(F_2)}})^T R^T_{F_2} R_{B_2} \end{array}\right] \tag{24}$$

2.1.3. Complete Jacobian of scleronomic constraints

The complete expression of the Jacobian matrix of constraint $C_{\boldsymbol{q}}$ is obtained by combining (15) and (24):

$$C_{\boldsymbol{q}} = \left[\begin{array}{c|c|c|c} R^T_{F_2} & -R^T_{F_2} R_{B_1} \widetilde{\boldsymbol{r}}_{F_{1\,(B_1)}} & -R^T_{F_2} & R^T_{F_2} R_{B_2} \widetilde{\boldsymbol{r}}_{F_{2\,(B_2)}} + R^T_{F_2} R_{B_2} \widetilde{\boldsymbol{r}12}_{(B_2)} \\ 0 & P(\boldsymbol{\rho}_{F_{1\,(F_2)}})^T R^T_{F_2} R_{B_1} & 0 & -P(\boldsymbol{\rho}_{F_{1\,(F_2)}})^T R^T_{F_2} R_{B_2} \end{array}\right] \tag{25}$$

Table 1
Several common joints inherited from the lock constraint.

	C_{q_x}	C_{q_y}	C_{q_z}	$C_{q_{Rx}}$	$C_{q_{Ry}}$	$C_{q_{Rz}}$
Fix	×	×	×	×	×	×
Coaxial		×	×		×	×
Prismatic		×	×	×	×	×
Revolute	×	×	×		×	×
Orthogonal				×		
Parallel					×	×
Plane	×				×	×
Spherical	×	×	×			
Distance along X	×					

that, for simplicity, we could rewrite emphasizing its six rows, the first three for the translational constraints and last three for the rotational constraints:

$$C_{\boldsymbol{q}}(\boldsymbol{q}) = \begin{bmatrix} C_{q_x} \\ C_{q_y} \\ C_{q_z} \\ C_{q_{Rx}} \\ C_{q_{Ry}} \\ C_{q_{Rz}} \end{bmatrix} \tag{26}$$

While the above general expression would constrain all six degrees of freedom between the two frames F_1 and F_2 it is indeed fairly easy to express other types of joints by just suppressing the corresponding rows according to the free DOFs, as reported in Table 1. The "×" symbol means the corresponding rows are active and thus the corresponding DOFs are constrained. For example, the Jacobian for a revolute joint along the x axis will have only five rows out of six, since the row corresponding to $C_{q_{Rx}}$ will be suppressed.

2.2. Rheonomic constraints

In the rheonomic constraint the relative motion of the driven frame F_1 with respect to the main frame F_2 is an explicit function of time $C(\boldsymbol{q}, t) = 0$. This case is often found while modelling linear or rotational actuators receiving a motion set-point from a controller.

2.2.1. Translational rheonomic constraints

The constraint equation of the rheonomic translational constraints can be expressed as:

$$\begin{aligned} \boldsymbol{C}(\boldsymbol{q}, t) &= \boldsymbol{r}_{F_1.F_{2(F_2)}} - \boldsymbol{r}_t = \\ &= R_{F_2}^T \left(\boldsymbol{r}_{B_1} + R_{B_1} \boldsymbol{r}_{F_{1(B_1)}} - \boldsymbol{r}_{B_2} - R_{B_2} \boldsymbol{r}_{F_{2(B_2)}} \right) - \boldsymbol{r}_t = \\ &= \boldsymbol{0}_{3\times 1} \end{aligned} \tag{27}$$

where $\boldsymbol{r}_t$ is the position vector corresponding to the relative translational motion of the driven frame F_1 with respect to the main frame F_2, which is specified by end users as a function of time.

The variation is derived as:

$$\delta \boldsymbol{C}(\boldsymbol{q}, t) = C_{\boldsymbol{q}} \delta \boldsymbol{q} + \boldsymbol{C}_t \delta t \tag{28}$$

where,

$$C_{\boldsymbol{q}} = \frac{\partial}{\partial \boldsymbol{q}} \left(R_{F_2}^T \left(\boldsymbol{r}_{B_1} + R_{B_1} \boldsymbol{r}_{F_{1(B_1)}} - \boldsymbol{r}_{B_2} - R_{B_2} \boldsymbol{r}_{F_{2(B_2)}} \right) \right) \tag{29a}$$

$$\boldsymbol{C}_t = -\frac{\partial \boldsymbol{r}_t}{\partial t} \tag{29b}$$

The rheonomic term $\boldsymbol{r}_t$ does not affect the computation of $C_{\boldsymbol{q}}$, leading to the same Jacobian matrix as (15).

2.2.2. Rotational rheonomic constraints

The constraint equation of the rheonomic rotational constraints is given as:

$$\boldsymbol{C}(\boldsymbol{q}, t) = -\mathrm{Im} \left(\boldsymbol{\rho}_t \boldsymbol{\rho}_{F_{2(F_1)}} \right) = \boldsymbol{0}_{3\times 1} \tag{30}$$

where $\boldsymbol{\rho}_t$ is the quaternion corresponding to the relative rotational motion of the driven frame F_1 with respect to the main frame F_2, which is specified by end users as a function of time. If the constraint is satisfied, there should be $\boldsymbol{\rho}_{F_1} = \boldsymbol{\rho}_{F_2} \boldsymbol{\rho}_t$.

By introducing a shadow frame $F_1^\diamond$ as $\boldsymbol{\rho}_{F_1^\diamond} = \boldsymbol{\rho}_{F_1}\boldsymbol{\rho}_t^*$ – where $\boldsymbol{\rho}^*$ denotes quaternion conjugate –, remembering the equality $\boldsymbol{\rho}_{F_{2(F_1)}} = \boldsymbol{\rho}^*_{F_1}\boldsymbol{\rho}_{F_2}$ and $\boldsymbol{\rho}^*_{F_{2(F_1)}} = \boldsymbol{\rho}_{F_{1(F_2)}}$, the constraint equation (30) can be rewritten as:

$$\boldsymbol{C}(\boldsymbol{q},t) = \mathrm{Im}\left(\boldsymbol{\rho}_{F_1^\diamond(F_2)}\right) = \boldsymbol{0}_{3\times1} \tag{31}$$

The shadow frame $F_1^\diamond$ is rotated back from the driven frame F_1 by the given rotation $\boldsymbol{\rho}_t$ to arrive at the same orientation as the main frame F_2. If the constraint is satisfied, the shadow frame $F_1^\diamond$ is coincident with the main frame F_2.

Similarly as the derivation from (18) to the results of (22) and (23), the variation of (31) is computed as:

$$\begin{aligned}\delta\boldsymbol{C}(\boldsymbol{q},t) &= P(\boldsymbol{\rho}_{F_1^\diamond(F_2)})\boldsymbol{R}^T_{F_1^\diamond}\left(\boldsymbol{R}_{B_1}\boldsymbol{\theta}^\delta_{l_{B_1}} - \boldsymbol{R}_{B_2}\boldsymbol{\theta}^\delta_{l_{B_2}}\right) = \\ &= P(\boldsymbol{\rho}_{F_1^\diamond(F_2)})^T\boldsymbol{R}^T_{F_2}\left(\boldsymbol{R}_{B_1}\boldsymbol{\theta}^\delta_{l_{B_1}} - \boldsymbol{R}_{B_2}\boldsymbol{\theta}^\delta_{l_{B_2}}\right)\end{aligned} \tag{32}$$

where the rheonomic term $\boldsymbol{C}_t = \frac{\partial}{\partial t}\left(\mathrm{Im}\left(\boldsymbol{\rho}_{F_1^\diamond(F_2)}\right)\right)$ does not affect $\boldsymbol{C}_{\boldsymbol{q}}$ and is not shown.

The complete expression of the Jacobian matrix of constraint $\boldsymbol{C}_{\boldsymbol{q}}(\boldsymbol{q},t)$ is obtained by replacing the blocks corresponding to the rotational DOFs in (25) with (32):

$$\boldsymbol{C}_{\boldsymbol{q}} = \left[\begin{array}{c|c|c|c} \boldsymbol{R}^T_{F_2} & -\boldsymbol{R}^T_{F_2}\boldsymbol{R}_{B_1}\widetilde{\boldsymbol{r}}_{F_{1(B_1)}} & -\boldsymbol{R}^T_{F_2} & \boldsymbol{R}^T_{F_2}\boldsymbol{R}_{B_2}\widetilde{\boldsymbol{r}}_{F_{2(B_2)}} + \boldsymbol{R}^T_{F_2}\boldsymbol{R}_{B_2}\widetilde{\boldsymbol{r}12}_{(B_2)} \\ \boldsymbol{0} & P(\boldsymbol{\rho}_{F_1^\diamond(F_2)})^T\boldsymbol{R}^T_{F_2}\boldsymbol{R}_{B_1} & \boldsymbol{0} & -P(\boldsymbol{\rho}_{F_1^\diamond(F_2)})^T\boldsymbol{R}^T_{F_2}\boldsymbol{R}_{B_2} \end{array}\right] \tag{33}$$

3. Tangent stiffness matrix of constraints

To derive the tangent stiffness matrix of constraints (10), one needs to linearize the reaction forces and torques $\boldsymbol{C}_{\boldsymbol{q}}(\boldsymbol{q},t)^T\boldsymbol{\gamma}$ with respect to the generalized coordinates $\delta\boldsymbol{q} = \left[\delta\boldsymbol{r}^T_{B_1}, \boldsymbol{\theta}^{\delta T}_{l_{B_1}}, \delta\boldsymbol{r}^T_{B_2}, \boldsymbol{\theta}^{\delta T}_{l_{B_2}}\right]^T$. The Lagrange multipliers $\boldsymbol{\gamma}$ are assumed constant in this linearization because their variations have been already included in the other linearization term $\boldsymbol{C}_{\boldsymbol{q}}(\boldsymbol{q},t)^T\delta\boldsymbol{\gamma}$ in (7).

3.1. Scleronomic constraint

3.1.1. Main part

The Lagrange multipliers $\boldsymbol{\gamma}$ can be split into two parts

$$\boldsymbol{\gamma} = \left[\boldsymbol{\gamma}^T_{f(F_2)}, \boldsymbol{\gamma}^T_{m(F_2)}\right]^T \tag{34}$$

where $\boldsymbol{\gamma}_{f_{(F_2)}}, \boldsymbol{\gamma}_{m_{(F_2)}} \in \mathbb{R}^3$ are the reaction forces and torques of the joint expressed in the main frame F_2, respectively.

Recalling the expression (25), the transpose of the Jacobian matrix of constraint can be written in the following compact form

$$\boldsymbol{C}^T_{\boldsymbol{q}} = \begin{bmatrix} \boldsymbol{J}^T_{x_1} & \boldsymbol{0} \\ \boldsymbol{J}^T_{r_1} & \boldsymbol{J}^T_{w_1} \\ \boldsymbol{J}^T_{x_2} & \boldsymbol{0} \\ \boldsymbol{J}^T_{r_2} & \boldsymbol{J}^T_{w_2} \end{bmatrix} \tag{35}$$

where the sub-blocks are

$$\boldsymbol{J}^T_{x_1} = \boldsymbol{R}_{F_2} \tag{36a}$$

$$\boldsymbol{J}^T_{r_1} = \widetilde{\boldsymbol{r}}_{F_{1(B_1)}}\boldsymbol{R}^T_{B_1}\boldsymbol{R}_{F_2} \tag{36b}$$

$$\boldsymbol{J}^T_{w_1} = \boldsymbol{R}^T_{B_1}\boldsymbol{R}_{F_2}P(\boldsymbol{\rho}_{F_{1(F_2)}}) \tag{36c}$$

$$\boldsymbol{J}^T_{x_2} = -\boldsymbol{R}_{F_2} \tag{36d}$$

$$\boldsymbol{J}^T_{r_2} = -\widetilde{\boldsymbol{r}}_{F_{2(B_2)}}\boldsymbol{R}^T_{B_2}\boldsymbol{R}_{F_2} - \widetilde{\boldsymbol{r}12}_{(B_2)}\boldsymbol{R}^T_{B_2}\boldsymbol{R}_{F_2} \tag{36e}$$

$$\boldsymbol{J}^T_{w_2} = -\boldsymbol{R}^T_{B_2}\boldsymbol{R}_{F_2}P(\boldsymbol{\rho}_{F_{1(F_2)}}) \tag{36f}$$

Since F_1, F_2 are rigidly attached on B_1, B_2 respectively, we have $\delta\boldsymbol{r}_{F_{1(B_1)}} = \boldsymbol{0}$, $\delta\boldsymbol{r}_{F_{2(B_2)}} = \boldsymbol{0}$, $\delta\boldsymbol{R}_{F_{1(B_1)}} = 0$, $\delta\boldsymbol{R}_{F_{2(B_2)}} = 0$. Meanwhile, remembering the equality $\delta\boldsymbol{R} = \boldsymbol{R}\widetilde{\boldsymbol{\theta}^\delta_l}$, and the property of the skew-symmetric matrix $\tilde{\boldsymbol{a}}^T = -\tilde{\boldsymbol{a}}, \forall\boldsymbol{a} \in \mathbb{R}^3$, the variations of the sub-blocks are calculated as

$$\delta\boldsymbol{J}^T_{x_1} = \boldsymbol{R}_{B_2}\widetilde{\boldsymbol{\theta}^\delta_{l\,B_2}}\boldsymbol{R}^T_{B_2}\boldsymbol{R}_{F_2} \tag{37a}$$

$$\delta\boldsymbol{J}^T_{r_1} = \widetilde{\boldsymbol{r}}_{F_{1(B_1)}}\left(-\widetilde{\boldsymbol{\theta}^\delta_{l\,B_1}}\boldsymbol{R}^T_{B_1}\boldsymbol{R}_{F_2} + \boldsymbol{R}^T_{B_1}\boldsymbol{R}_{B_2}\widetilde{\boldsymbol{\theta}^\delta_{l\,B_2}}\boldsymbol{R}^T_{B_2}\boldsymbol{R}_{F_2}\right) \tag{37b}$$

$$\delta\boldsymbol{J}^T_{w_1} = \left(-\widetilde{\boldsymbol{\theta}^\delta_{l\,B_1}}\boldsymbol{R}^T_{B_1}\boldsymbol{R}_{F_2} + \boldsymbol{R}^T_{B_1}\boldsymbol{R}_{B_2}\widetilde{\boldsymbol{\theta}^\delta_{l\,B_2}}\boldsymbol{R}^T_{B_2}\boldsymbol{R}_{F_2}\right)P(\boldsymbol{\rho}_{F_{1(F_2)}}) + \left(\boldsymbol{R}^T_{B_1}\boldsymbol{R}_{F_2}\right)\delta P(\boldsymbol{\rho}_{F_{1(F_2)}})$$

$$\delta J_{x_2}^T = -R_{B_2}\widetilde{\theta_{l_{B_2}}^{\delta}} R_{B_2}^T R_{F_2} \tag{37c}$$

$$\delta J_{r_2}^T = -\widetilde{\delta \boldsymbol{r}_{12_{(B_2)}}} R_{B_2}^T R_{F_2} \tag{37d}$$

$$\delta J_{w_2}^T = -R_{B_2}^T R_{F_2} \delta P(\boldsymbol{\rho}_{F_{1(F_2)}}) \tag{37e}$$

Recalling the definition of $\boldsymbol{r}_{12_{(B_2)}}$ in (14), and using the equalities $\tilde{\boldsymbol{a}}\boldsymbol{b} = -\tilde{\boldsymbol{b}}\boldsymbol{a}$, $\tilde{\boldsymbol{a}} + \tilde{\boldsymbol{b}} = \widetilde{\boldsymbol{a}+\boldsymbol{b}}$, $\forall \boldsymbol{a}, \boldsymbol{b} \in \mathbb{R}^3$, its variation $\delta \boldsymbol{r}_{12_{(B_2)}}$ is calculated as

$$\delta \boldsymbol{r}_{12_{(B_2)}} = R_{B_2}^T \delta \boldsymbol{r}_{B_1} - R_{B_2}^T R_{B_1} \tilde{\boldsymbol{r}}_{F_{1(B_1)}} \theta_{l_{B_1}}^{\delta} - R_{B_2}^T \delta \boldsymbol{r}_{B_2} + \left(\widetilde{\boldsymbol{r}_{12_{(B_2)}}} + \tilde{\boldsymbol{r}}_{F_{2(B_2)}} \right) \theta_{l_{B_2}}^{\delta} \tag{38}$$

Its skew-symmetric matrix is

$$\widetilde{\delta \boldsymbol{r}_{12_{(B_2)}}} = R_{B_2}^T \tilde{\delta \boldsymbol{r}}_{B_1} R_{B_2} - R_{B_2}^T R_{B_1} \left(\widetilde{\tilde{\boldsymbol{r}}_{F_{1(B_1)}} \theta_{l_{B_1}}^{\delta}} \right) R_{B_1}^T R_{B_2} - R_{B_2}^T \tilde{\delta \boldsymbol{r}}_{B_2} R_{B_2} + \left(\widetilde{\left(\widetilde{\boldsymbol{r}_{12_{(B_2)}}} + \tilde{\boldsymbol{r}}_{F_{2(B_2)}} \right) \theta_{l_{B_2}}^{\delta}} \right) \tag{39}$$

where the equalities $\widetilde{R\boldsymbol{r}} = R\tilde{\boldsymbol{r}}R^T, \forall R \in \mathrm{SO}(3), \boldsymbol{r} \in \mathbb{R}^3$ and $\tilde{\boldsymbol{a}} + \tilde{\boldsymbol{b}} = \widetilde{\boldsymbol{a}+\boldsymbol{b}}, \forall \boldsymbol{a},\ \boldsymbol{b} \in \mathbb{R}^3$ are used.

Substituting (39) into (37d), the calculation of $\delta J_{r_2}^T$ follows as

$$\delta J_{r_2}^T = -R_{B_2}^T \tilde{\delta \boldsymbol{r}}_{B_1} R_{F_2} + R_{B_2}^T R_{B_1} \left(\widetilde{\tilde{\boldsymbol{r}}_{F_{1(B_1)}} \theta_{l_{B_1}}^{\delta}} \right) R_{B_1}^T R_{F_2} + R_{B_2}^T \tilde{\delta \boldsymbol{r}}_{B_2} R_{F_2} - \left(\left(\widetilde{\boldsymbol{r}_{12_{(B_2)}}} + \widetilde{\tilde{\boldsymbol{r}}_{F_{2(B_2)}}} \right) \theta_{l_{B_2}}^{\delta} \right) R_{B_2}^T R_{F_2} \tag{40}$$

Recalling (34) and (35), the variation of the reaction forces and torques of the joint is expressed as

$$\delta C_{\boldsymbol{q}}^T \boldsymbol{\gamma} = \begin{bmatrix} \delta J_{x_1}^T \boldsymbol{\gamma}_{f_{(F_2)}} \\ \delta J_{r_1}^T \boldsymbol{\gamma}_{f_{(F_2)}} + \delta J_{w_1}^T \boldsymbol{\gamma}_{m_{(F_2)}} \\ \delta J_{x_2}^T \boldsymbol{\gamma}_{f_{(F_2)}} \\ \delta J_{r_2}^T \boldsymbol{\gamma}_{f_{(F_2)}} + \delta J_{w_2}^T \boldsymbol{\gamma}_{m_{(F_2)}} \end{bmatrix} \tag{41}$$

Substituting (37) and (40) into (41), and remembering the equalities $\widetilde{R\boldsymbol{r}} = R\tilde{\boldsymbol{r}}R^T, \forall R \in \mathrm{SO}(3), \boldsymbol{r} \in \mathbb{R}^3$ and $\tilde{\boldsymbol{a}}\boldsymbol{b} = -\tilde{\boldsymbol{b}}\boldsymbol{a}$, $\forall \boldsymbol{a}, \boldsymbol{b} \in \mathbb{R}^3$ from which follows the useful property $\widetilde{\theta_l^{\delta} R \boldsymbol{\gamma}} = -R\tilde{\boldsymbol{\gamma}} R^T \theta_l^{\delta}$, the four rows are calculated as

$$\delta J_{x_1}^T \boldsymbol{\gamma}_{f_{(F_2)}} = -R_{F_2} \widetilde{\boldsymbol{\gamma}_{f_{(F_2)}}} R_{F_2}^T R_{B_2} \theta_{l_{B_2}}^{\delta} \tag{42a}$$

$$\begin{aligned} \delta J_{r_1}^T \boldsymbol{\gamma}_{f_{(F_2)}} + \delta J_{w_1}^T \boldsymbol{\gamma}_{m_{(F_2)}} = {} & \tilde{\boldsymbol{r}}_{F_{1(B_1)}} R_{B_1}^T R_{F_2} \widetilde{\boldsymbol{\gamma}_{f_{(F_2)}}} R_{F_2}^T R_{B_1} \theta_{l_{B_1}}^{\delta} - \tilde{\boldsymbol{r}}_{F_{1(B_1)}} R_{B_1}^T R_{F_2} \widetilde{\boldsymbol{\gamma}_{f_{(F_2)}}} R_{F_2}^T R_{B_2} \theta_{l_{B_2}}^{\delta} \\ & + R_{B_1}^T R_{F_2} \left(\widetilde{P(\boldsymbol{\rho}_{F_{1(F_2)}}) \boldsymbol{\gamma}_{m_{(F_2)}}} \right) R_{F_2}^T R_{B_1} \theta_{l_{B_1}}^{\delta} - R_{B_1}^T R_{F_2} \left(\widetilde{P(\boldsymbol{\rho}_{F_{1(F_2)}}) \boldsymbol{\gamma}_{m_{(F_2)}}} \right) R_{F_2}^T R_{B_2} \theta_{l_{B_2}}^{\delta} \\ & + R_{B_1}^T R_{F_2} \delta P(\boldsymbol{\rho}_{F_{1(F_2)}}) \boldsymbol{\gamma}_{m_{(F_2)}} \end{aligned} \tag{42b}$$

$$\delta J_{x_2}^T \boldsymbol{\gamma}_{f_{(F_2)}} = R_{F_2} \widetilde{\boldsymbol{\gamma}_{f_{(F_2)}}} R_{F_2}^T R_{B_2} \theta_{l_{B_2}}^{\delta} \tag{42c}$$

$$\begin{aligned} \delta J_{r_2}^T \boldsymbol{\gamma}_{f_{(F_2)}} + \delta J_{w_2}^T \boldsymbol{\gamma}_{m_{(F_2)}} = {} & R_{B_2}^T R_{F_2} \widetilde{\boldsymbol{\gamma}_{f_{(F_2)}}} R_{F_2}^T \delta \boldsymbol{r}_{B_1} - R_{B_2}^T R_{F_2} \widetilde{\boldsymbol{\gamma}_{f_{(F_2)}}} R_{F_2}^T \delta \boldsymbol{r}_{B_2} \\ & - R_{B_2}^T R_{F_2} \widetilde{\boldsymbol{\gamma}_{f_{(F_2)}}} R_{F_2}^T R_{B_1} \tilde{\boldsymbol{r}}_{F_{1(B_1)}} \theta_{l_{B_1}}^{\delta} + R_{B_2}^T R_{F_2} \widetilde{\boldsymbol{\gamma}_{f_{(F_2)}}} R_{F_2}^T R_{B_2} \left(\widetilde{\boldsymbol{r}_{12_{(B_2)}}} + \tilde{\boldsymbol{r}}_{F_{2(B_2)}} \right) \theta_{l_{B_2}}^{\delta} \\ & - R_{B_2}^T R_{F_2} \delta P(\boldsymbol{\rho}_{F_{1(F_2)}}) \boldsymbol{\gamma}_{m_{(F_2)}} \end{aligned} \tag{42d}$$

Substituting (42) into (41), and grouping the coefficient terms according to the generalized coordinates $\delta \boldsymbol{q} = \left[\delta \boldsymbol{r}_{B_1}^T, \boldsymbol{\theta}_{l_{B_1}}^{\delta T}, \delta \boldsymbol{r}_{B_2}^T, \boldsymbol{\theta}_{l_{B_2}}^{\delta T} \right]^T$, one obtains

$$\delta C_{\boldsymbol{q}}^T \boldsymbol{\gamma} = K_c^{(M)} \delta \boldsymbol{q} + \delta \Gamma \tag{43}$$

where the main part of the tangent stiffness matrix of constraints is

$$K_c^{(M)} = \begin{bmatrix} 0 & 0 & 0 & K_{c_{14}}^{(M)} \\ 0 & K_{c_{22}}^{(M)} & 0 & K_{c_{24}}^{(M)} \\ 0 & 0 & 0 & K_{c_{34}}^{(M)} \\ K_{c_{41}}^{(M)} & K_{c_{42}}^{(M)} & K_{c_{43}}^{(M)} & K_{c_{44}}^{(M)} \end{bmatrix} \tag{44}$$

of which the sub-blocks are

$$K_{c_{14}}^{(M)} = -R_{F_2} \widetilde{\boldsymbol{\gamma}_{f_{(F_2)}}} R_{F_2}^T R_{B_2} \tag{45a}$$

$$K_{c_{22}}^{(M)} = \tilde{\boldsymbol{r}}_{F_{1(B_1)}} R_{B_1}^T R_{F_2} \widetilde{\boldsymbol{\gamma}_{f_{(F_2)}}} R_{F_2}^T R_{B_1} + R_{B_1}^T R_{F_2} \left(\widetilde{P(\boldsymbol{\rho}_{F_{1(F_2)}}) \boldsymbol{\gamma}_{m_{(F_2)}}} \right) R_{F_2}^T R_{B_1} \tag{45b}$$

$$K_{c_{24}}^{(M)} = -\tilde{\boldsymbol{r}}_{F_{1(B_1)}} R_{B_1}^T R_{F_2} \widetilde{\boldsymbol{\gamma}_{f_{(F_2)}}} R_{F_2}^T R_{B_2} - R_{B_1}^T R_{F_2} \left(\widetilde{P(\boldsymbol{\rho}_{F_{1(F_2)}}) \boldsymbol{\gamma}_{m_{(F_2)}}} \right) R_{F_2}^T R_{B_2} \tag{45c}$$

$$K_{c_{34}}^{(M)} = R_{F_2}\widetilde{\boldsymbol{\gamma}}_{f_{(F_2)}}R_{F_2}^T R_{B_2} \tag{45d}$$

$$K_{c_{41}}^{(M)} = R_{B_2}^T R_{F_2}\widetilde{\boldsymbol{\gamma}}_{f_{(F_2)}}R_{F_2}^T \tag{45e}$$

$$K_{c_{42}}^{(M)} = -R_{B_2}^T R_{F_2}\widetilde{\boldsymbol{\gamma}}_{f_{(F_2)}}R_{F_2}^T R_{B_1}\tilde{\boldsymbol{r}}_{F_{1(B_1)}} \tag{45f}$$

$$K_{c_{43}}^{(M)} = -R_{B_2}^T R_{F_2}\widetilde{\boldsymbol{\gamma}}_{f_{(F_2)}}R_{F_2}^T \tag{45g}$$

$$K_{c_{44}}^{(M)} = R_{B_2}^T R_{F_2}\widetilde{\boldsymbol{\gamma}}_{f_{(F_2)}}R_{F_2}^T R_{B_2}\left(\widetilde{\boldsymbol{r}12}_{(B_2)} + \tilde{\boldsymbol{r}}_{F_{2(B_2)}}\right) \tag{45h}$$

The remaining part of (43) is

$$\delta\Gamma = \begin{bmatrix} 0 \\ R_{B_1}^T R_{F_2}\delta P(\boldsymbol{\rho}_{F_{1(F_2)}})\boldsymbol{\gamma}_{m_{(F_2)}} \\ 0 \\ -R_{B_2}^T R_{F_2}\delta P(\boldsymbol{\rho}_{F_{1(F_2)}})\boldsymbol{\gamma}_{m_{(F_2)}} \end{bmatrix} \tag{46}$$

When F_1 and F_2 are coincident, for instance when the constraint of the fixed joint is satisfied, the relative quaternion $\boldsymbol{\rho}_{F_{1(F_2)}}$ is the identity quaternion, and the projection matrix boils down to $P(\boldsymbol{\rho}_{F_{1(F_2)}}) = \frac{1}{2}I_{3\times3}$.

3.1.2. Projection part

The matrix $P(\boldsymbol{\rho}_{F_{1(F_2)}})$ present in (25) – originated from the variation of the quaternion of (C.2) – can map the Lagrange multipliers $\boldsymbol{\gamma}_{m_{(F_2)}}$ to a part of the reaction torques in the basis of the main frame F_2, thus we call it *projection matrix*. Consequently, the remaining term (46) is called the *projection part* of the tangent stiffness matrix of constraints.

Remembering the equality (C.12), and substituting (21), the expression (46) is further derived as

$$\delta\Gamma = \begin{bmatrix} 0 \\ R_{B_1}^T R_{F_2} G\left(\boldsymbol{\rho}_{F_{1(F_2)}}, \boldsymbol{\gamma}_{m_{(F_2)}}\right) R_{F_1}^T\left(R_{B_1}\theta_{l_{B_1}}^{\delta} - R_{B_2}\theta_{l_{B_2}}^{\delta}\right) \\ 0 \\ -R_{B_2}^T R_{F_2} G\left(\boldsymbol{\rho}_{F_{1(F_2)}}, \boldsymbol{\gamma}_{m_{(F_2)}}\right) R_{F_1}^T\left(R_{B_1}\theta_{l_{B_1}}^{\delta} - R_{B_2}\theta_{l_{B_2}}^{\delta}\right) \end{bmatrix} \tag{47}$$

Grouping the coefficient terms according to the generalized coordinates $\delta\boldsymbol{q} = \left[\delta\boldsymbol{r}_{B_1}^T, \theta_{l_{B_1}}^{\delta T}, \delta\boldsymbol{r}_{B_2}^T, \theta_{l_{B_2}}^{\delta T}\right]^T$, one obtains the projection part of the tangent stiffness matrix of constraints as

$$K_c^{(P)} = \begin{bmatrix} 0 & 0 & 0 & 0 \\ 0 & K_{c_{22}}^{(P)} & 0 & K_{c_{24}}^{(P)} \\ 0 & 0 & 0 & 0 \\ 0 & K_{c_{42}}^{(P)} & 0 & K_{c_{44}}^{(P)} \end{bmatrix} \tag{48}$$

of which the sub-blocks are

$$K_{c_{22}}^{(P)} = R_{B_1}^T R_{F_2} G\left(\boldsymbol{\rho}_{F_{1(F_2)}}, \boldsymbol{\gamma}_{m_{(F_2)}}\right) R_{F_1}^T R_{B_1} \tag{49a}$$

$$K_{c_{24}}^{(P)} = -R_{B_1}^T R_{F_2} G\left(\boldsymbol{\rho}_{F_{1(F_2)}}, \boldsymbol{\gamma}_{m_{(F_2)}}\right) R_{F_1}^T R_{B_2} \tag{49b}$$

$$K_{c_{42}}^{(P)} = -R_{B_2}^T R_{F_2} G\left(\boldsymbol{\rho}_{F_{1(F_2)}}, \boldsymbol{\gamma}_{m_{(F_2)}}\right) R_{F_1}^T R_{B_1} \tag{49c}$$

$$K_{c_{44}}^{(P)} = R_{B_2}^T R_{F_2} G\left(\boldsymbol{\rho}_{F_{1(F_2)}}, \boldsymbol{\gamma}_{m_{(F_2)}}\right) R_{F_1}^T R_{B_2} \tag{49d}$$

If F_1, F_2 are coincident, for instance, when the constraint of the fixed joint is satisfied, the relative quaternion $\boldsymbol{\rho}_{F_{1(F_2)}}$ is the identity quaternion, one has a simple matrix $G\left(\boldsymbol{\rho}_{F_{1(F_2)}}, \boldsymbol{\gamma}_{m_{(F_2)}}\right) = -\frac{1}{4}\widetilde{\boldsymbol{\gamma}}_{m_{(F_2)}}$.

3.1.3. Complete form

The complete form of the tangent stiffness matrix of constraints is the summation of the main part (44) and the projection part (48).

$$K_c = K_c^{(M)} + K_c^{(P)} \tag{50}$$

The block patterns of $K_c^{(M)}$ and $K_c^{(P)}$ are symmetric, but in general both of them are neither symmetric nor skew-symmetric.

The tangent stiffness matrix of constraints of other types of joints in Table 1 can be calculated using (50) directly. The reaction forces and torques associated with the free DOFs are zero, thus the corresponding rows can be removed from the Jacobian matrix of constraints.

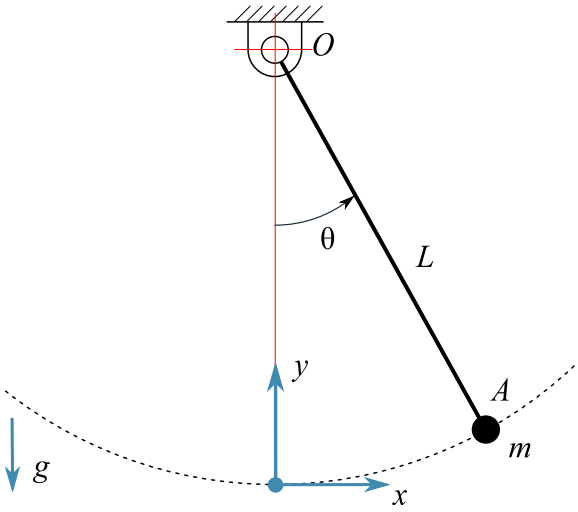

Fig. 2. The pendulum with a point mass, hinged at one end of the link under gravity.

3.2. Rheonomic constraints

The Jacobian matrix of translational rheonomic constraints is the same as the scleronomic constraints, hence the tangent stiffness matrix is the same.

There is a difference in the rotational rheonomic constraints. By comparing the expression (25) and (33), one can note that the only discrepancy between the scleronomic and rheonomic constraints is the projection matrix P: replacing $P(\boldsymbol{\rho}_{F_{1(F_2)}})$ in (25) with $P(\boldsymbol{\rho}_{F_1^{\diamond}(F_2)})$ one obtains the expression (33). Thus one just needs to replace $P(\boldsymbol{\rho}_{F_{1(F_2)}})$ in (44) with $P(\boldsymbol{\rho}_{F_1^{\diamond}(F_2)})$ to revise the main part of the tangent stiffness matrix of the rheonomic constraint and replace the quaternion $\boldsymbol{\rho}_{F_{1(F_2)}}$ with $\boldsymbol{\rho}_{F_1^{\diamond}(F_2)}$ in (47) to obtain the projection part of the tangent stiffness matrix of the rheonomic constraint.

4. Examples

In order to emphasize the main role of the tangent stiffness matrix of constraints both in static and eigenvalue analyses a set of examples are chosen and modelled in the open-source multibody software Chrono [16]. The high flexibility of the tool allows to selectively enable and disable the stiffness term on the base of the required testing conditions.

4.1. Pendulum

The pendulum example consists of a single point mass hinged at the top point O to the fixed world and has an initial offset angle θ with respect to the vertical axis i.e. to the gravity direction (see Fig. 2 and Table 2). A Newton–Raphson iteration loop is performed in the initial configuration to search for a set of generalized coordinates $\boldsymbol{q}$ and Lagrange multipliers $\boldsymbol{\gamma}$ satisfying all the constraints under the external forces. After this *assembling* phase, reaction forces and torques of the joints are determined, thus allowing the correct evaluation of the tangent stiffness matrix of constraints ((45) and (49)). By suppressing the inertia and damping forces in (7), a Newton–Raphson iteration loop is then carried out to find the *static* equilibrium. The mass, stiffness, damping matrices and the Jacobian matrix of constraints of the system are extracted in this latter equilibrium configuration. The generalized eigenvalue problem [1] is set up and the eigenvalues are solved.

When the mass starts in a lower position with respect to the hinge point O ($\|\theta\| < 90$ deg) the static analysis converges to the lowest equilibrium configuration. In this case, the eigenvalues are a pair of imaginary numbers 0 ± 1.566i which indicates the oscillating behaviour of the pendulum, matching the theoretical value $\omega = \sqrt{g/L} = 1.566$ rad s^{-1}. In contrast, when the mass of the pendulum starts above the hinge point O ($\|\theta\| > 90$ deg), the pendulum converges to the upper (unstable) equilibrium state. This is an expected behaviour of the Newton–Raphson iteration that looks for the closest solution. The eigenvalues are a pair of real numbers $\pm 1.566 + 0$i thus implying an unstable motion; their absolute values match the theoretical solution.

Without the tangent stiffness matrix of constraints, the system stiffness matrix of the pendulum becomes zero, leading to the failure of static and eigenvalue analyses.

In order to test the computational workload introduced by the evaluation of the K_c term, the pendulum dynamic simulation has been run for $t_{\text{sim}} = 1 \times 10^4$ s on an Intel Core(R) i7 10510U CPU, with 1.80 GHz and 16 GB of RAM; the Intel VTune(R) tool has been used for profiling. The total required CPU time resulted in $t_{\text{cpu}} = 12.632$ s, of which 1.124 s (i.e. 8.9%), were spent in the evaluation of the tangent stiffness matrix of constraints.

Table 2
Pendulum parameters.

Property	Value
Mass (m)	15 kg
Length (L)	4 m
Gravity acceleration (g)	9.81 m s^{-2}
Offset angle (θ)	30°

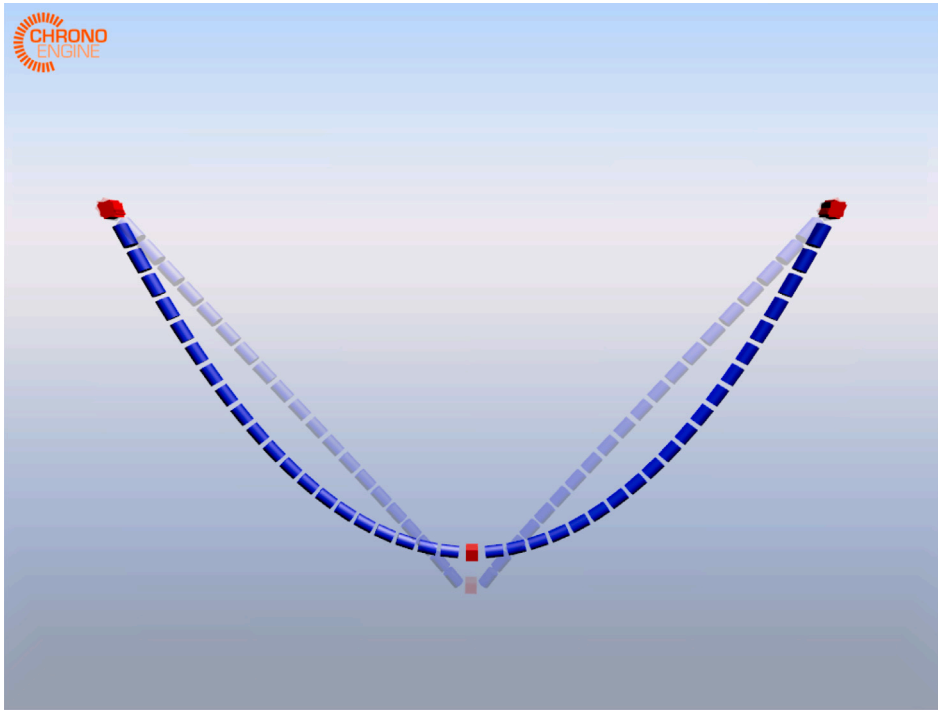

Fig. 3. An anchor chain hinged at two ends under gravity in its initial and equilibrium configuration.

4.2. Anchor chain

An anchor chain is modelled using a series of rigid bodies and joints (Fig. 3). The left and right ends of the anchor chain are hinged at the coordinates $A(0,0,0)$ and $B(10,0,0)$. The middle point is given at $C(5,0,-6)$. A series of rigid bodies connected through double revolute joints (where the two bending degrees of freedom are released) are built between A, C, and B, C and initialized in a 'V' shape configuration. The axial flexibility of the chain is neglected since the interest is to investigate the effect of the tangent stiffness matrix of constraints. Nevertheless, the inextensibility hypothesis is a good approximation from the practical point of view [17].

4.2.1. Static analysis

The assembly and static analyses are carried out. The anchor chain drops because of gravity, as shown in Fig. 3. The horizontal components of the reaction forces of the joints expressed in the absolute frame are found to be constant, which is a typical characteristic of the catenary curve.

The analytical expression of a catenary curve is $z = a\cosh(x/a + x_0) + z_0$, where x_0, z_0 are the coordinate offsets of the original point, $a = T_0/(mg)$ is the constant coefficient of the catenary curve, T_0 is the horizontal internal force, m is the mass per unit length and g is the gravity acceleration.

The coordinates of the rigid bodies on the anchor chain in the equilibrium configuration are compared against the analytical catenary curve, as Fig. 4.

4.2.2. Eigenvalue analysis

Also the eigenvalue analysis of the anchor chain at the equilibrium state is performed. The modal frequencies of the first four modes are listed in Table 3, where the corresponding modal shapes are plotted in Fig. 5.

Non-linear time domain simulations are performed to identify the first four modal frequencies. A constant force $\boldsymbol{f}$ is applied at the point C in the first 5 s to excite the vibration of the anchor chain around the equilibrium state. Later the force is removed to

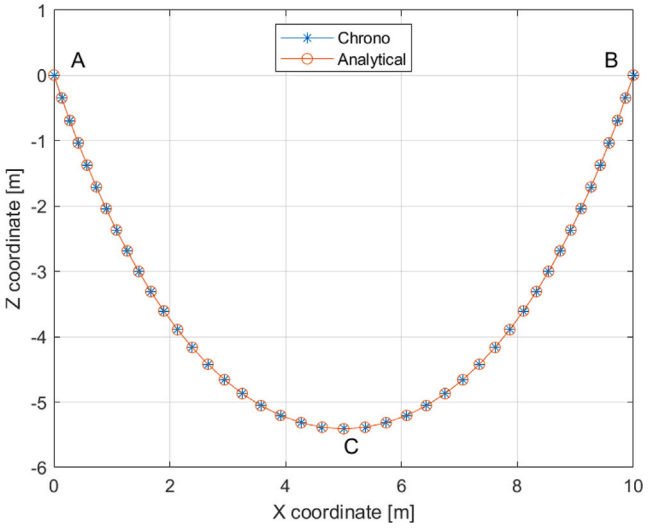

Fig. 4. The validation of the catenary curve.

Table 3
Modal frequencies of the anchor chain.

No.	Frequency [Hz]
1	0.240
2	0.309
3	0.504
4	0.551

allow the free vibration. The amplitude spectrum from FFT analysis is shown in Fig. 6, where the data of the first 10 s have been discarded to avoid the influence of the transient impulse at the beginning of the simulation.

The constant force is applied in the X (longitudinal), Y (lateral), and Z (vertical) directions, respectively, to activate the vibration of the corresponding modes:

- When the excitation force $\boldsymbol{f}$ is applied in the $+X$ direction, as in Fig. 6(a), the anchor chain oscillates at the frequency 0.311 Hz, which matches the second modal frequency in Table 3.
- When the excitation force $\boldsymbol{f}$ is applied in the $+Y$ direction, as in Fig. 6(b), the dominant frequency is 0.244 Hz, whereas another peak frequency of 0.544 Hz is also observed with a lower amplitude. These two peak frequencies match the first and fourth modal frequencies in Table 3, respectively.
- When the excitation force $\boldsymbol{f}$ is applied in the $-Z$ direction, as in Fig. 6(c), the anchor chain oscillates at the frequency 0.5 Hz, which corresponds to the third modal frequency in Table 3.

The oscillation follows the directions of the excitation forces in the aforementioned three test cases, and is consistent with the dominant directions of the corresponding modal shapes. It is concluded that a pretty good agreement is obtained between the eigenvalue analysis and the non-linear time domain simulations.

4.3. Double wishbone suspension

The double-wishbone suspension proposed in [11] has been replicated (Fig. 7) preserving the original geometry and inertial properties, but replacing some of the original constraints:

- the wheel has been considered as a rigid body and fixed to the upright;
- the non-holonomic constraint between the tyre and the road has been removed;
- the chassis has been fixed with respect to ground;
- the suspension damper has been excluded from the simulation, in order to get the undamped vibration modes;
- the excitation force is applied along the vertical direction directly to the wheel;
- since only few specifications were given about the spring–damper, the preload compression has been set to 4275 N, leading to a rest length of 0.664 m.

With this setup the equilibrium force to be applied to the wheel centre resulted in $F_0 = 3253$ N.

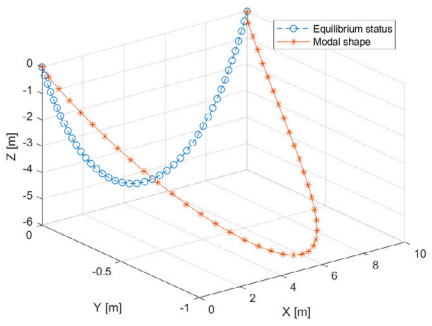

(a) *No.1, out-of-plane swinging mode.*

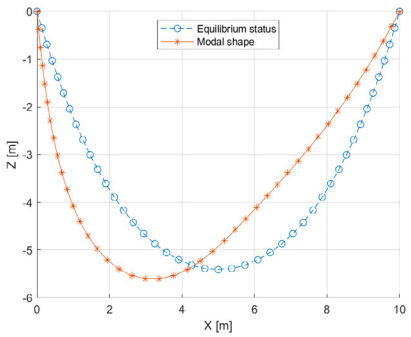

(b) *No.2, in-plane swinging mode.*

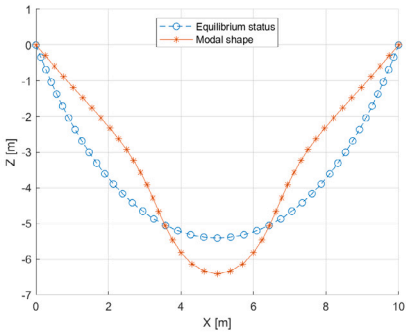

(c) *No.3, in-plane bending mode.*

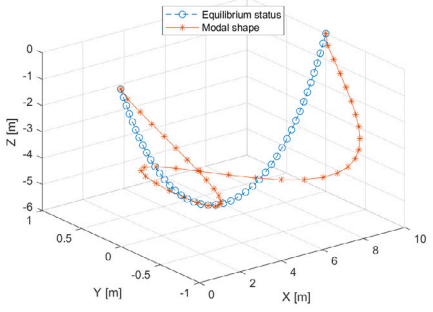

(d) *No.4, out-of-plane bending mode.*

Fig. 5. Modal shapes of the anchor chain.

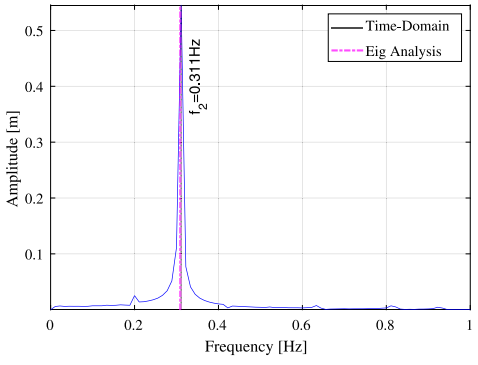

(a) *In-Plane horizontal vibration.*

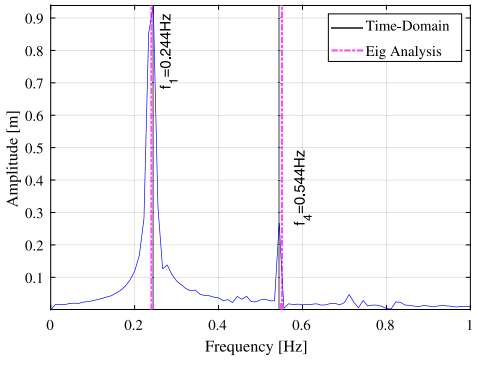

(b) *out-of-plane vibration.*

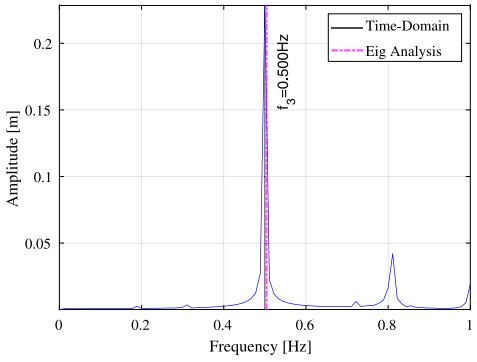

(c) *In-Plane vertical vibration.*

Fig. 6. The vibration of the middle point C of the anchor chain.

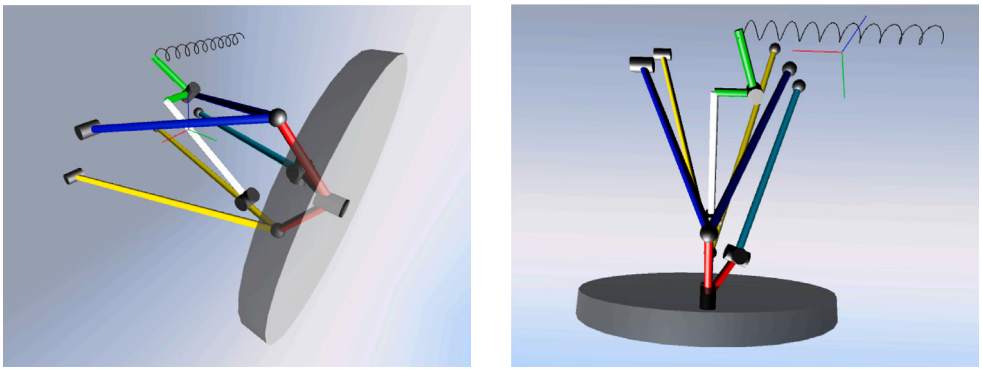

(a) *Side View.* (b) *Top View.*

Fig. 7. Double Wishbone Suspension.

This setup has been used, with little variations, for all the three different analyses. Summarizing: the suspension is initially analysed through a time-domain dynamic simulation by applying a modest perturbation force to the wheel hub. The oscillations are then analysed in the frequency domain and the results compared against the eigenvalue solution. This approach is indeed reasonable since the dynamic simulation is not affected by the tangent stiffness matrix of constraints, thus allowing the fairest comparison. Eigenvalues of the structure, with and without the tangent stiffness matrix of constraints are then compared.

In more detail, during the time-domain simulation an additional excitation force is temporarily added to the system. The force is applied right at the beginning of the simulation in the vertical direction, with a magnitude of 1% of the equilibrium preload F_0 and released as a step function at $t = 1\,\mathrm{s}$. The simulation runs for $t = 50\,\mathrm{s}$ with a timestep of $\Delta t = 1\,\mathrm{ms}$; this guarantees the required resolution and frequency span for the Fourier analysis; the Hilbert-Hughes-Taylor integrator method (HHT) is used in order to reduce the numerical damping effects.

The time signal of the vertical position (suspension travel) is transformed by the Fast Fourier Transform in MATLAB in its frequency-domain equivalent. An appropriate window has been applied in order to filter out the perturbation phase. Fig. 8 shows the resulting spectrum: the main mode at frequency $3.799\,\mathrm{Hz}$ is clearly identified.

The second term for the comparison comes from the eigenvalue solution of the structure. Again, a preliminary assembly phase, followed by a static simulation is required to make the system reach the correct initial configuration. In this phase the tangent stiffness matrix of constraints *has* to be included since it is crucial for the proper convergence of the model. In the next step two eigenvalue analyses are run, both *with* and *without* K_c. Since the tangent stiffness matrix of constraints is asymmetric the Krylov-Schur eigenvalue solver has been used.

Results coming from the two eigenvalue analyses are compared with those coming from the dynamic simulation, taken as reference value. The results highlight relevant differences: the frequency obtained including the tangent stiffness matrix of constraints ($3.899\,\mathrm{Hz}$) shows a significantly closer match compared to the results where the K_c matrix has been neglected ($3.125\,\mathrm{Hz}$). It has to be noted that the choice of different integration schemes might matter: picking HHT over simpler Implicit Euler methods allows to reduce the shifting effect of the damping, in any case always below 2%.

5. Conclusion

Using quaternion-based finite rotations, we derived a general expression of holonomic constraint equations and their Jacobian matrix. The formulation represents a generic fixed joint, but it can be easily extended to a series of derived free-motion joints by suppressing specific rows of the Jacobian matrix. Also, a consistent and unified analytical expression for the tangent stiffness matrix of constraints is derived, showing the split between two (asymmetric) terms $K_c = K_c^{(M)} + K_c^{(P)}$.

Three examples are presented to demonstrate the importance of K_c in the static and eigenvalue analyses of multibody dynamics systems featuring rigid-body motions.

The analytical expression of the tangent stiffness matrix of holonomic constraints has been implemented in the open-source multibody library CHRONO [16].

Declaration of competing interest

The authors declare that they have no known competing financial interests or personal relationships that could have appeared to influence the work reported in this paper.

Data availability

Data will be made available on request.

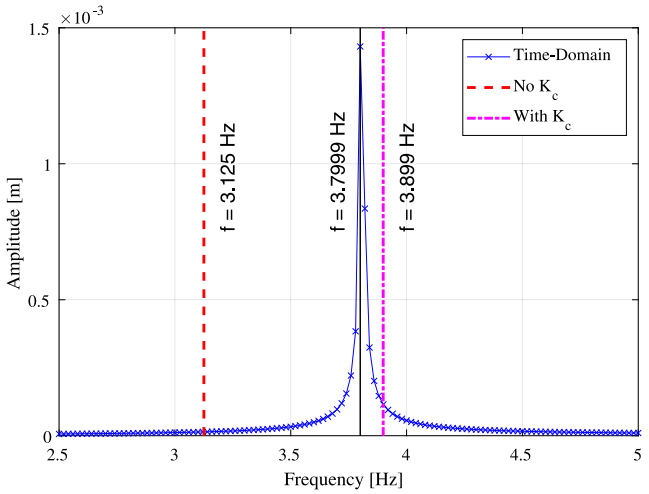

Fig. 8. Frequency of free degree of motion.

Appendix A. Notation

Here is the generic convention that we use for symbols.

In some cases, for rotations and displacements or their derivatives, we need to specify respect to which reference frames they are expressed, and in which basis they are measured. This is done using subscripts like in the following scheme

$$\square_{\mathrm{TO.FROM_{(BASIS)}}}$$

where FROM can be a point of the origin of a frame, TO can be a point or the origin of a frame, (BASIS) is a frame.

For some tensorial quantities (virtual rotation vectors, position vectors, etc.) we often use *l* or *a* as shorthand symbols for (BASIS), where *l* means measured in the *local* basis (also *intrinsic* or *material quantities*, in some literatures), *a* means measured in the absolute basis or in general in the parent basis (also known as *extrinsic* or *spatial quantities*, in some literatures).

When there are no sources of misunderstanding, we omit or simplify those subscripts as in the following examples, where one understands that if the TO entity is omitted, it is assumed to be the (BASE) entity, and if also the (BASE) entity is omitted, then it is assumed to be the W world reference.

t	time
$\boldsymbol{q}$	vector of configurations
$\boldsymbol{\rho}$	rotation (quaternion) of a rigid body frame
$\boldsymbol{r}_{B.A_{(C)}}$	position of B respect to A, in C basis
$\boldsymbol{r}_{B_{(A)}}$	position of B respect to A, in B basis
$\boldsymbol{r}_A$	position of A respect to W world reference, in W basis
$R_{A_{(B)}}$	rotation matrix of frame A respect to frame B
R_A	rotation matrix of frame A respect to world reference, shorthand for $R_{A_{(W)}}$
$\boldsymbol{\theta}^{\delta}_{a_A}$	virtual rotation vector of frame A respect to absolute world reference, in *absolute* basis, shorthand for $\boldsymbol{\theta}^{\delta}_{A.W_{(W)}}$ or $\boldsymbol{\theta}^{\delta}_{A_{(W)}}$
$\boldsymbol{\theta}^{\delta}_{l_A}$	virtual rotation vector of frame A respect to absolute world reference, in *local* basis, shorthand for $\boldsymbol{\theta}^{\delta}_{A.W_{(A)}}$ or $\boldsymbol{\theta}^{\delta}_{A_{(A)}}$

Appendix B. Rotation parametrization via quaternions

While important properties and definitions for quaternions can be easily found in literature (for example [18,19]), more specific symbols and properties used in the paper are listed in this section.

The variation of the identity quaternion $\boldsymbol{\rho}_I = [1,0,0,0]^T$ is equal to the zero quaternion $\boldsymbol{\rho}_0 = [0,0,0,0]^T$

$$\delta\boldsymbol{\rho}\boldsymbol{\rho}^* + \boldsymbol{\rho}\delta\boldsymbol{\rho}^* = \delta\boldsymbol{\rho}^*\boldsymbol{\rho} + \boldsymbol{\rho}^*\delta\boldsymbol{\rho} = \boldsymbol{\rho}_0 \tag{B.1}$$

The unit quaternion $\boldsymbol{\rho}$ can be used to operate a rotation of a vector in the three–dimensional space

$$(0, \boldsymbol{r}_a) = \boldsymbol{\rho}(0, \boldsymbol{r}_l)\boldsymbol{\rho}^* \tag{B.2}$$

where $\boldsymbol{r}_l$, $\boldsymbol{r}_a$ are the vectors expressed in the local and parent frames, respectively.

The rotation transformation (B.2) can be also performed via a rotation tensor $R \in \mathrm{SO}(3)$ as

$$\boldsymbol{r}_a = R\boldsymbol{r}_l \tag{B.3}$$

where the rotation matrix R can be computed from its corresponding quaternion $\boldsymbol{\rho}$ as

$$R(\boldsymbol{\rho}) = \begin{bmatrix} \rho_0^2+\rho_1^2-\rho_2^2-\rho_3^2 & 2(\rho_1\rho_2-\rho_3\rho_0) & 2(\rho_1\rho_3+\rho_2\rho_0) \\ 2(\rho_1\rho_2+\rho_3\rho_0) & \rho_0^2-\rho_1^2+\rho_2^2-\rho_3^2 & 2(-\rho_1\rho_0+\rho_2\rho_3) \\ 2(\rho_1\rho_3-\rho_2\rho_0) & 2(\rho_1\rho_0+\rho_2\rho_3) & \rho_0^2-\rho_1^2-\rho_2^2+\rho_3^2 \end{bmatrix} \tag{B.4}$$

The rotation matrix $R(\boldsymbol{\rho})$ can be also expressed as a product of two auxiliary matrices $F(q)_\oplus$ and $F(q)_\ominus$ as

$$R(\boldsymbol{\rho}) = F(\boldsymbol{\rho})_\oplus F(\boldsymbol{\rho})_\ominus{}^T \tag{B.5a}$$

$$F(\boldsymbol{\rho})_\oplus = \begin{bmatrix} +\rho_1 & +\rho_0 & -\rho_3 & +\rho_2 \\ +\rho_2 & +\rho_3 & +\rho_0 & -\rho_1 \\ +\rho_3 & -\rho_2 & +\rho_1 & +\rho_0 \end{bmatrix} \tag{B.5b}$$

$$F(\boldsymbol{\rho})_\ominus = \begin{bmatrix} +\rho_1 & +\rho_0 & +\rho_3 & -\rho_2 \\ +\rho_2 & -\rho_3 & +\rho_0 & +\rho_1 \\ +\rho_3 & +\rho_2 & -\rho_1 & +\rho_0 \end{bmatrix} \tag{B.5c}$$

These two auxiliary matrices have the following properties, that hold only for the unit quaternion $\boldsymbol{\rho}$

$$F(\boldsymbol{\rho})_\oplus F(\boldsymbol{\rho})_\oplus{}^T = F(\boldsymbol{\rho})_\ominus F(\boldsymbol{\rho})_\ominus{}^T = I \tag{B.6a}$$

$$F(\boldsymbol{\rho})_\oplus{}^T F(\boldsymbol{\rho})_\oplus = F(\boldsymbol{\rho})_\ominus{}^T F(\boldsymbol{\rho})_\ominus = (I - \boldsymbol{\rho}^*\boldsymbol{\rho}^{*T}) \tag{B.6b}$$

The variation of (B.2) follows the chain rule as

$$(0, \delta\boldsymbol{r}_a) = \delta\boldsymbol{\rho}(0, \boldsymbol{r}_l)\boldsymbol{\rho}^* + \boldsymbol{\rho}(0, \boldsymbol{r}_l)\delta\boldsymbol{\rho}^* + \boldsymbol{\rho}(0, \delta\boldsymbol{r}_l)\boldsymbol{\rho}^* \tag{B.7}$$

Remembering the equality $\delta R = R\widetilde{\theta_l^\delta}$, the variation of the vector $\delta\boldsymbol{r}_a$ can be also performed for the rotation transformation (B.3)

$$\delta\boldsymbol{r}_a = \delta R\boldsymbol{r}_l + R\delta\boldsymbol{r}_l = R\widetilde{\theta_l^\delta}\boldsymbol{r}_l + R\delta\boldsymbol{r}_l \tag{B.8}$$

where θ_l^δ is the *virtual rotation vector*[1] in the local basis. $\widetilde{(\,)}$ is the operator to convert a vector to its corresponding skew-symmetric matrix.

Expanding (B.8) to the notation of pure quaternions, and remembering the equivalent rotation transformation via the quaternion in (B.2) and the rotation tensor in (B.3), one obtains

$$(0, \delta\boldsymbol{r}_a) = \boldsymbol{\rho}(0, \widetilde{\theta_l^\delta}\boldsymbol{r}_l)\boldsymbol{\rho}^* + \boldsymbol{\rho}(0, \delta\boldsymbol{r}_l)\boldsymbol{\rho}^* \tag{B.9}$$

Substituting (B.9) into (B.7), and making use of the property (B.1), one obtains

$$(0, \widetilde{\theta_l^\delta}\boldsymbol{r}_l) = \boldsymbol{\rho}^*\delta\boldsymbol{\rho}(0, \boldsymbol{r}_l) - (0, \boldsymbol{r}_l)\boldsymbol{\rho}^*\delta\boldsymbol{\rho} \tag{B.10}$$

From (B.1) one sees the summation of $\boldsymbol{\rho}^*\delta\boldsymbol{\rho}$ and its conjugate is ρ_0, thus $\boldsymbol{\rho}^*\delta\boldsymbol{\rho}$ is a pure quaternion and can be denoted as $\boldsymbol{\rho}^*\delta\boldsymbol{\rho} = (0, \boldsymbol{\nu}_\Delta)$. After removing the zero real part, (B.10) can be simplified as

$$\widetilde{\theta_l^\delta}\boldsymbol{r}_l = 2\widetilde{\boldsymbol{\nu}_\Delta}\boldsymbol{r}_l \tag{B.11}$$

The equality (B.11) is true for an arbitrary vector $\boldsymbol{r}_l$, leading to a concise equation $\theta_l^\delta = 2\boldsymbol{\nu}_\Delta$. Expanding it to pure quaternions, one obtains the transformation relation between the variation of a rotation quaternion $\delta\boldsymbol{\rho}$ and its corresponding virtual rotation vector θ_l^δ

$$\delta\boldsymbol{\rho} = \frac{1}{2}\boldsymbol{\rho}(0, \theta_l^\delta) \tag{B.12a}$$

$$\delta\boldsymbol{\rho} = \frac{1}{2}(0, \boldsymbol{\theta}_a^\delta)\boldsymbol{\rho}^* \tag{B.12b}$$

where θ_a^δ is the virtual rotation vector expressed in the parent frame, $\theta_a^\delta = R(\rho)\theta_l^\delta$.

As an alternative, by using matrix algebra, and remembering (B.5) and (B.6), one can express (B.12) as

$$\delta\boldsymbol{\rho} = \frac{1}{2}F(\boldsymbol{\rho}^*)_\oplus{}^T\boldsymbol{\theta}_l^\delta \tag{B.13a}$$

$$\delta\boldsymbol{\rho} = \frac{1}{2}F(\boldsymbol{\rho}^*)_\ominus{}^T\boldsymbol{\theta}_a^\delta \tag{B.13b}$$

[1] In general, θ^δ is not the differential of an Euclidean vector θ. In practical terms, there is no way to obtain a finite θ by directly integrating a vector $\delta\theta$. This is the reason why we prefer the notation θ^δ instead of $\delta\theta$ to avoid misunderstandings.

Appendix C. Projection matrix

By introducing a projection matrix $P(\boldsymbol{\rho}) \in \mathbb{R}^{3\times3}$ equal to the bottom three rows of the matrix $\frac{1}{2}F(\boldsymbol{\rho}^*)_{\oplus}{}^T$, which can be expressed as

$$P(\boldsymbol{\rho}) = \frac{1}{2}\left(sI_{3\times3} + \tilde{\boldsymbol{v}}\right) \tag{C.1}$$

the imaginary vectorial part of (B.13a) can be written as

$$\mathrm{Im}\left(\delta\boldsymbol{\rho}\right) = P(\boldsymbol{\rho})\boldsymbol{\theta}_l^{\delta} \tag{C.2}$$

The projection matrix $P(\boldsymbol{\rho})$ of a unit quaternion $\boldsymbol{\rho}$ has important properties as below

$$P(\boldsymbol{\rho})^T = P(\boldsymbol{\rho}^*) \tag{C.3a}$$

$$P(\boldsymbol{\rho}) = P(\boldsymbol{\rho})^T R(\boldsymbol{\rho}) \tag{C.3b}$$

$$P(\boldsymbol{\rho}) = R(\boldsymbol{\rho})^T P(\boldsymbol{\rho}) R(\boldsymbol{\rho}) \tag{C.3c}$$

$$P(\boldsymbol{\rho})^{-1} = \frac{1}{s}\left(R(\boldsymbol{\rho})^T + I_{3\times3}\right) \tag{C.3d}$$

When the rotation angle represented by $\boldsymbol{\rho}$ is $\pm\pi$, the scalar part $s = 0$, leading to a singular projection matrix $P(\boldsymbol{\rho})$.

For the quaternion $\boldsymbol{\rho}_{F_{1(F_2)}}$ representing the relative rotation of the driven frame F_1 with respect to the main frame F_2, remembering (C.3b), and expanding the relative rotation $R(\boldsymbol{\rho}_{F_{1(F_2)}}) = R_{F_2}^T R_{F_1}$, one obtains

$$P(\boldsymbol{\rho}_{F_{1(F_2)}})^T R_{F_2}^T = P(\boldsymbol{\rho}_{F_{1(F_2)}}) R_{F_1}^T \tag{C.4}$$

For an arbitrary unit quaternion $\boldsymbol{\rho} = (s, \boldsymbol{v})$, its variation can be denoted as

$$\delta\boldsymbol{\rho} = (\delta s, \delta\boldsymbol{v}) \tag{C.5}$$

Recalling the equality (B.12a), and remembering the multiplication properties, the variation of a quaternion can be computed as

$$\delta\boldsymbol{\rho} = \frac{1}{2}(s, \boldsymbol{v})\left(0, \boldsymbol{\theta}_l^{\delta}\right) = \frac{1}{2}\left(-\boldsymbol{v}\cdot\boldsymbol{\theta}_l^{\delta}, s\boldsymbol{\theta}_l^{\delta} + \boldsymbol{v}\times\boldsymbol{\theta}_l^{\delta}\right) \tag{C.6}$$

where $(\cdot)$ is the dot product of two vectors, and $(\times)$ is the cross product of two vectors.

Comparing (C.5) and (C.6), the scalar and vectorial parts of the variations should be equal respectively, leading to

$$\delta s = -\frac{1}{2}\boldsymbol{v}\cdot\boldsymbol{\theta}_l^{\delta} \tag{C.7}$$

$$\delta\boldsymbol{v} = \frac{1}{2}\left(s\boldsymbol{\theta}_l^{\delta} + \boldsymbol{v}\times\boldsymbol{\theta}_l^{\delta}\right) \tag{C.8}$$

Remembering the definition of the projection matrix (C.1), after substituting (C.7) and (C.8), and using the equalities $\tilde{\boldsymbol{a}} + \tilde{\boldsymbol{b}} = \widetilde{\boldsymbol{a}+\boldsymbol{b}}$, $\widetilde{\tilde{\boldsymbol{a}}\boldsymbol{b}} = \tilde{\boldsymbol{a}}\check{\boldsymbol{b}} - \check{\boldsymbol{b}}\tilde{\boldsymbol{a}}, \forall \boldsymbol{a}, \boldsymbol{b} \in \mathbb{R}^3$, the variation of the projection matrix $P(\boldsymbol{\rho})$ can be derived as

$$\delta P(\boldsymbol{\rho}) = \frac{1}{4}\left(-\left(\boldsymbol{v}\cdot\boldsymbol{\theta}_l^{\delta}\right) I_{3\times3} + \left(sI_{3\times3} + \tilde{\boldsymbol{v}}\right)\widetilde{\boldsymbol{\theta}_l^{\delta}} - \widetilde{\boldsymbol{\theta}_l^{\delta}}\tilde{\boldsymbol{v}}\right) \tag{C.9}$$

Its multiplication with Lagrange multipliers $\boldsymbol{\gamma}_m$ can be further calculated as

$$\delta P(\boldsymbol{\rho})\boldsymbol{\gamma}_m = \left(-\frac{1}{4}\boldsymbol{\gamma}_m\boldsymbol{v}^T - \frac{1}{4}\widetilde{\boldsymbol{\gamma}_m}\left(sI_{3\times3} + \tilde{\boldsymbol{v}}\right)\right)\boldsymbol{\theta}_l^{\delta} \tag{C.10}$$

where the equalities $(\boldsymbol{a}\cdot\boldsymbol{b})\boldsymbol{c} = \left(\boldsymbol{c}\boldsymbol{a}^T\right)\boldsymbol{b}$, $\tilde{\boldsymbol{a}}\boldsymbol{b} = -\tilde{\boldsymbol{b}}\boldsymbol{a}$, $\widetilde{\tilde{\boldsymbol{a}}\boldsymbol{b}} = \tilde{\boldsymbol{a}}\check{\boldsymbol{b}} - \check{\boldsymbol{b}}\tilde{\boldsymbol{a}}$, $\forall \boldsymbol{a}, \boldsymbol{b}, \boldsymbol{c} \in \mathbb{R}^3$ are used.

By introducing another auxiliary matrix $G\left(\boldsymbol{\rho}, \boldsymbol{\gamma}_m\right) \in \mathbb{R}^{3\times3}$

$$G\left(\boldsymbol{\rho}, \boldsymbol{\gamma}_m\right) = -\frac{1}{4}\boldsymbol{\gamma}_m\boldsymbol{v}^T - \frac{1}{4}\widetilde{\boldsymbol{\gamma}_m}\left(sI_{3\times3} + \tilde{\boldsymbol{v}}\right) \tag{C.11}$$

one obtains an equality in a compact form

$$\delta P(\boldsymbol{\rho})\boldsymbol{\gamma}_m = G\left(\boldsymbol{\rho}, \boldsymbol{\gamma}_m\right)\boldsymbol{\theta}_l^{\delta} \tag{C.12}$$

References

[1] D. Mangoni, A. Tasora, C. Peng, Complex eigenvalue analysis of multibody problems via sparsity-preserving krylov-Schur iterations, Machines (ISSN: 2075-1702) 11 (2) (2023) http://dx.doi.org/10.3390/machines11020218, URL https://www.mdpi.com/2075-1702/11/2/218.

[2] A. Lopez, I. Puente, H. Aizpurua, Experimental and analytical studies on the rotational stiffness of joints for single-layer structures, Eng. Struct. (ISSN: 0141-0296) 33 (3) (2011) 731–737, http://dx.doi.org/10.1016/j.engstruct.2010.11.023, URL https://www.sciencedirect.com/science/article/pii/S0141029610004438.

[3] E. Eich-Soellner, C. Führer, Numerical Methods in Multibody Dynamics, Vol. 45, Springer, 1998.

[4] M. Tournier, M. Nesme, B. Gilles, F. Faure, Stable constrained dynamics, ACM Trans. Graph. 34 (2015) http://dx.doi.org/10.1145/2766969.

[5] S. Andrews, M. Teichmann, P. Kry, Geometric stiffness for real-time constrained multibody dynamics, Comput. Graph. Forum 36 (2017) 235–246, http://dx.doi.org/10.1111/cgf.13122.
[6] M. Macklin, K. Erleben, M. Müller, N. Chentanez, S. Jeschke, V. Makoviychuk, Non-smooth Newton methods for deformable multi-body dynamics, ACM Trans. Graph. (ISSN: 0730-0301) 38 (5) (2019) 140:1–140:20, http://dx.doi.org/10.1145/3338695.
[7] D. Negrut, J. Ortiz, A practical approach for the linearization of the constrained multibody dynamics equations, J. Comput. Nonlinear Dyn. 1 (2006) http://dx.doi.org/10.1115/1.2198876.
[8] F. González, P. Masarati, J. Cuadrado, M.A. Naya, Assessment of linearization approaches for multibody dynamics formulations, J. Comput. Nonlinear Dyn. (ISSN: 1555-1415) 12 (4) (2017) http://dx.doi.org/10.1115/1.4035410.
[9] O. Bauchau, Flexible Multibody Dynamics, in: Solid mechanics and its applications, Springer, ISBN: 9789400703353, 2010, URL http://books.google.com/books?id=Pn94Czlg7VUC.
[10] M. Géradin, A. Cardona, Flexible Multibody Dynamics: A Finite Element Approach, Vol. 4, first ed., Wiley, ISBN: 978-0-471-48990-0, 2001.
[11] B. Minaker, The tangent stiffness matrix in rigid multibody vehicle dynamics, Math. Comput. Model. Dyn. Syst. 21 (3) (2014) 288–310, http://dx.doi.org/10.1080/13873954.2014.953549, arXiv:10.1080/13873954.2014.953549.
[12] B. Minaker, The tangent stiffness matrix of a constant velocity joint, in: 2021 CCToMM Mechanisms, Machines, and Mechatronics (M^3) Symposium.
[13] A.A. Shabana, Dynamics of Multibody Systems, Fourth, Cambridge University Press, Cambridge, England, 2013.
[14] A. Tasora, M. Anitescu, A matrix-free cone complementarity approach for solving large-scale, nonsmooth, rigid body dynamics, Comput. Methods Appl. Mech. Engrg. (ISSN: 0045-7825) 200 (5–8) (2011) 439–453, http://dx.doi.org/10.1016/j.cma.2010.06.030, URL http://www.sciencedirect.com/science/article/B6V29-50GWN46-2/2/47d6da2ab8348d986a3f57335006bfae.
[15] A. Tasora, P. Righettini, Application of quaternion algebra to the efficient computation of Jacobians for holonomic-rheonomic constraints, in: Advances in Computational Multibody Dynamics, IDMEC/IST, Lisbon, Portugal, 1999.
[16] A. Tasora, R. Serban, H. Mazhar, A. Pazouki, D. Melanz, J. Fleischmann, M. Taylor, H. Sugiyama, D. Negrut, Chrono: An open source multi-physics dynamics engine, in: T. Kozubek (Ed.), High Performance Computing in Science and Engineering, Springer, 2016, pp. 19–49.
[17] C. Pesce, A. Fujarra, A. Simos, E. Tannuri, Analytical and closed form solutions for deep water riser-like eigenvalue problem, in: International Ocean and Polar Engineering Conference, All Days, 1999, ISOPE-I-99-154, arXiv:https://onepetro.org/ISOPEIOPEC/proceedings-pdf/ISOPE99/All-ISOPE99/ISOPE-I-99-154/1927347/isope-i-99-154.pdf.
[18] D. Holm, Geometric Mechanics-Part II: Rotating, Translating and Rolling, World Scientific, 2011.
[19] G. Legnani, I. Fassi, A. Tasora, D. Fusai, A practical algorithm for smooth interpolation between different angular positions, Mech. Mach. Theory (ISSN: 0094-114X) 162 (2021) 104341, http://dx.doi.org/10.1016/j.mechmachtheory.2021.104341, URL https://www.sciencedirect.com/science/article/pii/S0094114X21000999.